JOURNAL OF PETROLOGY | VOLUME 49 | NUMBER 3 | PAGES 493–522 | 2008 | doi:10.1093/petrology/egm090

Petrogenesis of Cogenetic Silica-Oversaturated and -Undersaturated Syenites by Periodic Recharge in a Crustally Contaminated Magma Chamber: the Kangerlussuaq Intrusion, East Greenland

MORTEN S. RIISHUUS[1]*, DAVID W. PEATE[2], CHRISTIAN TEGNER[1], J. RICHARD WILSON[1] AND C. KENT BROOKS[3]

[1]DEPARTMENT OF EARTH SCIENCES, UNIVERSITY OF AARHUS, 8000 ÅRHUS C, DENMARK

[2]DEPARTMENT OF GEOSCIENCE, UNIVERSITY OF IOWA, 121 TROWBRIDGE HALL, IOWA CITY, IA 52242, USA

[3]GEOLOGICAL INSTITUTE, UNIVERSITY OF COPENHAGEN, ØSTER VOLDGADE 10, 1350 COPENHAGEN K, DENMARK

RECEIVED DECEMBER 2, 2004; ACCEPTED DECEMBER 27, 2007
ADVANCE ACCESS PUBLICATION JANUARY 30, 2008

The Palaeogene Kangerlussuaq Intrusion (~50 Ma) of East Greenland displays concentric zonation from quartz-rich nordmarkite (quartz syenite) at the margin, through pulaskite, to foyaite (nepheline syenite) in the centre; modal layering and igneous lamination are locally developed but there are no internal intrusive contacts. This is an apparent violation of the phase relations in Petrogeny's Residua System. We propose that this intrusion is layered, grading from quartz syenite at the bottom to nepheline syenite at the top. Mineral and whole-rock major and trace element data and Sr–Nd–Hf–Pb isotope data are presented that provide constraints on the petrogenesis of the intrusion. Radiogenic isotope data indicate a continuously decreasing crustal component from the quartz nordmarkites ($^{87}Sr/^{86}Sr = 0{\cdot}7061$; $\varepsilon_{Ndi} = 2{\cdot}3$; $\varepsilon_{Hfi} = 5{\cdot}2$; $^{206}Pb/^{204}Pb_{meas} = 16{\cdot}98$) to the foyaites ($^{87}Sr/^{86}Sr = 0{\cdot}7043$–$0{\cdot}7044$; $\varepsilon_{Ndi} = 3{\cdot}8$–$4{\cdot}9$; $\varepsilon_{Hfi} = 10{\cdot}7$–$11{\cdot}1$; $^{206}Pb/^{204}Pb_{meas} = 17{\cdot}78$–$17{\cdot}88$); the foyaites are dominated by a mantle isotopic signature. The average Mg-number of amphibole cores becomes increasingly primitive, varying from 26·4 in the nordmarkites to 57·4 in the pulaskites. Modal layering, feldspar lamination and the presence of huge basaltic xenoliths derived from the chamber roof, now resting on the transient chamber floor, demonstrate bottom-upwards crystallization. The intrusion cannot, therefore, have formed in a system closed to magmatic recharge. The lack of gneissic xenoliths in the nordmarkites suggests that most contamination took place deeper in the crust. In the proposed model, the nordmarkitic magma formed during crustal assimilation in the roof zone of a large, silica-undersaturated alkali basaltic/basanitic, stratified magma chamber, prior to emplacement in the uppermost crust. The more primitive syenites, terminating with foyaite at the top of the intrusion, formed as a consequence of repeated recharge of the Kangerlussuaq Intrusion magma chamber by tapping less contaminated, more primitive phonolitic melt from deeper parts of the underlying chamber during progressive armouring of the plumbing system.

KEY WORDS: *Kangerlussuaq; East Greenland; syenite; crustal contamination; magma mixing*

INTRODUCTION

Processes leading to the formation of cogenetic quartz and nepheline syenites have been a long-standing issue in petrological research because of the presence of a thermal barrier (Ab–Or join) between them in Petrogeny's Residua System (Ne–Ks–Q–H_2O). Liquidus phase

*Corresponding author. Present address: Department of Geological and Environmental Sciences, Stanford University, Stanford, CA 94305, USA. Telephone: +1 650 723 0841. Fax: +1 650 723 2199. E-mail: riishuus@stanford.edu

relations in this simple system imply that a melt will fractionate either towards the granite minimum and give rise to silica-oversaturated rocks, or towards the nepheline syenite minimum and give rise to silica-undersaturated rocks (Schairer, 1950; Tuttle & Bowen, 1958; Fudali, 1963; Hamilton & MacKenzie, 1965).

Mechanisms suggested to allow for generation of cogenetic over- and undersaturated rocks are: (1) processes that overcome or remove the thermal barrier, involving volatiles (Kogarko, 1974), increasing water pressure (Pankhurst *et al.*, 1976), or crystal fractionation (Foland & Henderson, 1976; Giret *et al.*, 1980); (2) open-system processes in which undersaturated magmas undergo assimilation of silica-rich crustal material and fractional crystallization (AFC) or produce oversaturated anatectic crustal melts (Brooks & Gill, 1982; Fitton, 1987). Increasing support has recently been given to open-system processes, as first proposed by Brooks & Gill (1982) (e.g. Foland *et al.*, 1993; Harris, 1995; Harris *et al.*, 1999; Marks *et al.*, 2003). Foland *et al.* (1993) presented data from the complexes of Marangudzi, Zimbabwe, and Mt. Brome, southern Quebec, characterized by cogenetic quartz and nepheline syenites, which showed that the undersaturated rocks have low Sr isotopic ratios and high Nd isotopic ratios, whereas the oversaturated syenites have high Sr isotopic ratios and low Nd isotopic ratios, indicating that these rocks originated from a felsic, undersaturated magma subjected to open-system crustal contamination processes. Using phase equilibrium constraints, and assuming that the required heat for assimilation is balanced by the latent heat of crystallization with no cooling of the magma, Foland *et al.* (1993) calculated model liquid AFC and fractional crystallization paths from an undersaturated melt. They concluded that closed-system fractional crystallization will produce only silica-undersaturated melts, whereas silica-oversaturated melts require crustal contamination processes.

The Kangerlussuaq Intrusion is an important example of syenitic magma that appears to have differentiated across the thermal barrier between silica-oversaturated and -undersaturated compositions (Wager, 1965), in apparent violation of phase relations in Petrogeny's Residua System (Schairer, 1950). Unlike most alkaline complexes with coexisting quartz and nepheline syenites (e.g. the Ilímaussaq, Marangudzi and Mt. Brome complexes), the Kangerlussuaq Intrusion has no internal intrusive contacts, but displays a gradual transition from quartz syenite to nepheline syenite. In this paper we present comprehensive mineral, major and trace element whole-rock and Sr–Nd–Hf–Pb isotopic data for a suite of samples from the Kangerlussuaq Intrusion and evaluate the magmatic processes that can produce a close association of silica-oversaturated and -undersaturated syenites.

GEOLOGICAL BACKGROUND

Regional geology and geochronology

The Kangerlussuaq Intrusion (KI) is situated within the East Greenland volcanic rifted margin and belongs to the Palaeogene North Atlantic Igneous Province (e.g. Saunders *et al.*, 1997) (Fig. 1). The East Greenland tholeiitic lavas and gabbroic intrusions can be divided into two discrete phases: (1) the earliest volcanics, including the Lower Basalts (Nielsen *et al.*, 1981), Nansen Fjord (Larsen *et al.*, 1989) and Urbjerget formations (Hansen *et al.*, 2002) at 61–58 Ma, which have been related to plume impact under Central Greenland; (2) the voluminous tholeiitic Plateau Basalts (e.g. Larsen *et al.*, 1989; Pedersen *et al.*, 1997; Tegner *et al.*, 1998*b*) at 56–55 Ma (Storey *et al.*, 2007), possibly erupted in just 300 kyr (Larsen & Tegner, 2006), which represent decompressional melting during continental break-up (Tegner *et al.*, 1998*a*). This activity is followed by younger events, dominantly at 50–47 Ma but extending to 37–35 Ma (Tegner *et al.*, 2008) and 14–13 Ma (Storey *et al.*, 2004), with production of mainly gabbroic and syenitic intrusions (e.g. Nielsen, 1987; Bernstein *et al.*, 1998) that post-date the initiation of sea-floor spreading, and are inferred to be caused by the passage of the rifted margin over the Iceland plume axis (Tegner *et al.*, 1998*a*, 2008).

The alkaline magmatism of the Kangerlussuaq area is volumetrically dominated by the Kangerlussuaq Alkaline Complex, which includes the KI (Wager, 1965; Kempe & Deer, 1970, 1976; Kempe *et al.*, 1970; Pankhurst *et al.*, 1976; Brooks & Gill, 1982) plus a series of older and younger satellite intrusions (e.g. Deer & Kempe, 1976; Holm & Prægel, 1988, 2006; Nielsen, 2002; Riishuus *et al.*, 2005, 2006) (Fig. 1b). The KI has been dated by several techniques. Beckinsale *et al.* (1970) dated a transitional pulaskite by the K–Ar method to $50{\cdot}4 \pm 1{\cdot}2$ Ma. Pankhurst *et al.* (1976) reported two Rb–Sr ages: $49{\cdot}9 \pm 1{\cdot}0$ Ma (biotite/feldspar/titanite) and $50{\cdot}0 \pm 1{\cdot}9$ Ma (whole-rock). Gleadow & Brooks (1979) reported zircon ($50{\cdot}8 \pm 1{\cdot}8$ Ma) and titanite ($51{\cdot}1 \pm 2{\cdot}8$ Ma) fission-track ages. Tegner *et al.* (2008) dated biotite from a pulaskite to $50{\cdot}8 \pm 1{\cdot}1$ Ma using ^{40}Ar–^{39}Ar.

The Kangerlussuaq Intrusion

The KI was discovered by L. R. Wager during the British Arctic Air Route Expedition in 1930. The intrusion was subsequently described in three papers that focused on its form and structure (Wager, 1965), petrology (Kempe *et al.*, 1970) and mineralogy (Kempe & Deer, 1970).

The KI is roughly circular with a diameter of 30–35 km ($\sim$800 km^2), which makes it the largest exposed Palaeogene intrusion in East Greenland and one of the largest syenitic intrusions in world. To the authors' knowledge the Brandberg Complex (Schmitt *et al.*, 2000), and Khibina and Lovozero centres (e.g. Kramm & Kogarko, 1994) are

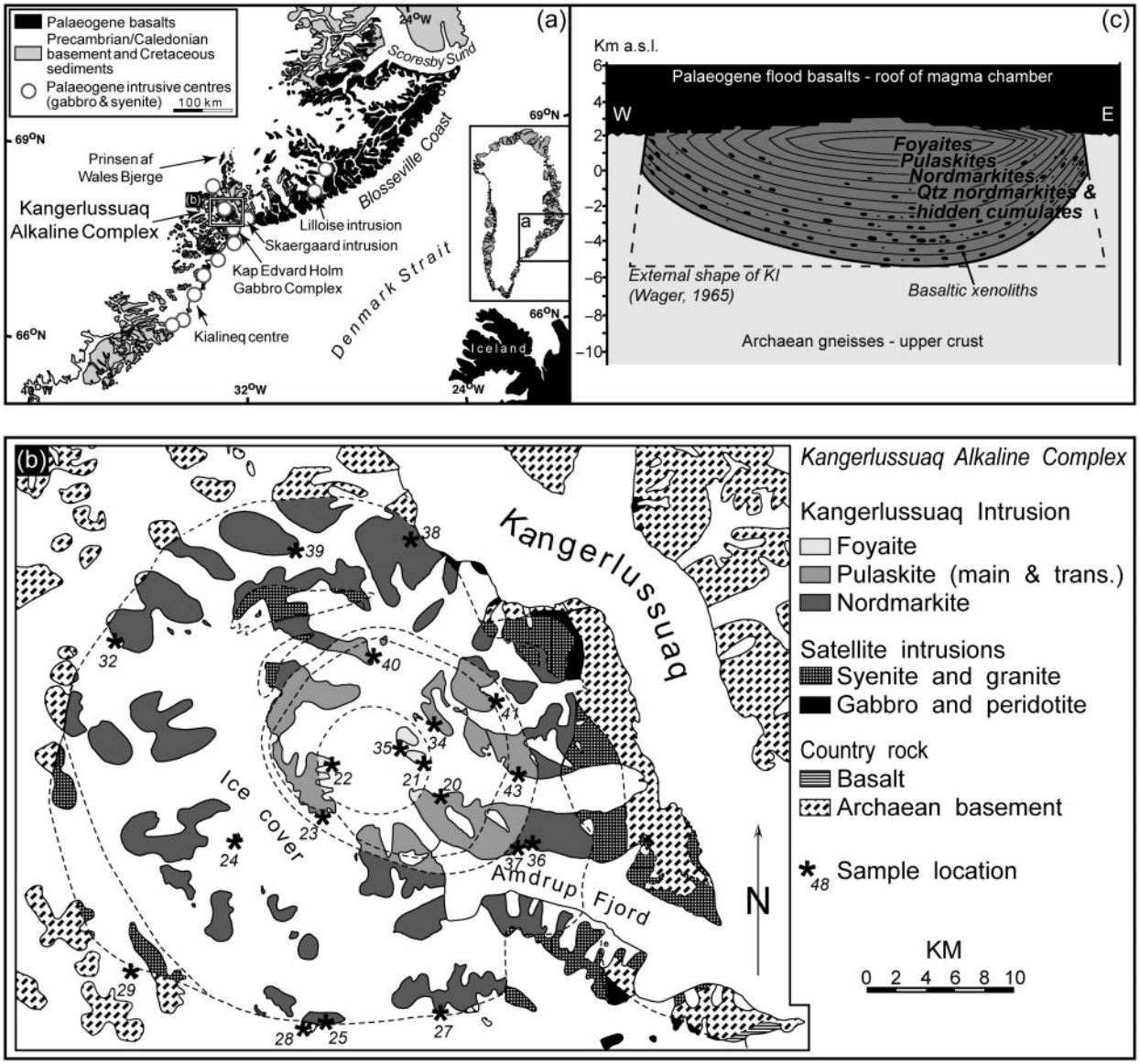

Fig. 1. (a) Map of Central East Greenland showing the distribution of Palaeogene flood basalts, intrusive centres (gabbros and syenites) and the Precambrian and Caledonian basement. (b) Map of the Kangerlussuaq Alkaline Complex west of Kangerlussuaq Fjord (after Kempe *et al.*, 1970). Sample locations are indicated by asterisks. (c) Hypothetical cross-section west to east of the Kangerlussuaq Intrusion, modified after Wager (1965).

the only other evolved intrusions of comparable size and similar setting. The KI grades from foyaites (>5% feldspathoids) in the centre, through main pulaskites (<5% feldspathoids) and transitional pulaskites (neither quartz nor feldspathoids), into nordmarkites (<10% quartz) and outermost quartz nordmarkites (~10% quartz) (Wager, 1965) (Fig. 1b). Wager (1965) argued that the gradual transition between the units indicates only a single pulse of magma injection. Based on field relations, especially the presence of trains of basaltic xenoliths, from the quartz nordmarkites through the outer part of the main pulaskites, dipping 30–60° towards the centre (Fig. 2a) and igneous lamination in the form of platy feldspars (Fig. 3c) dipping similarly inwards, Wager (1965) visualized the three-dimensional shape of the intrusion as resembling a pile of saucers with a decreasing diameter inwards and upwards through the succession and an assumed horizontal base, which gave an estimated volume of ~6500 km^3 (Fig. 1c). He showed that the intrusion was emplaced at the unconformity between the Archaean basement and the overlying flood basalts, and had stoped into the lava pile. We propose a modification of Wager's model

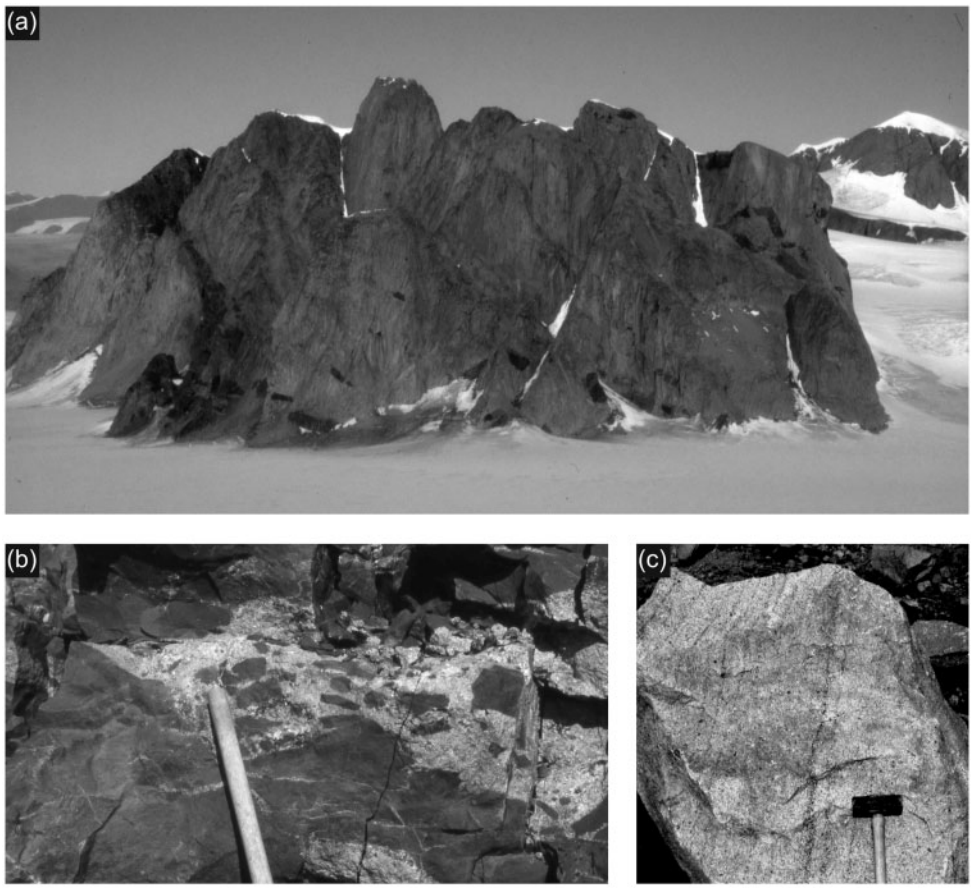

Fig. 2. (a) Southwest face of nunatak at location 32 (Fig. 1b) with quartz nordmarkites of the Kangerlussuaq Intrusion hosting dark trains of basaltic xenoliths visible in left- and right-hand side of picture. The nunatak rises 600–800 m above the glacial plateau at ~1000 m elevation. (b) Xenolith of basalt [from base of nunatak shown in (a)] invaded, brecciated and veined by quartz nordmarkite. The hammer shaft is ~30 cm long. (c) Layering in quartz nordmarkite defined by the planar concentration of FeMg-silicates. The hammer head is ~10 cm wide.

shape by suggesting an asymmetric, saucer-shaped base (Fig. 1c), not unlike the 'classical' funnel shape suggested for many large intrusions, which reduces the volume to ~4000 km^3. The field evidence of basaltic xenoliths and platy feldspars along with the relationship of nordmarkites being cut by nepheline-bearing pegmatites whereas the foyaites are not cut by quartz-bearing aplites and pegmatites, led Wager (1965) to regard the KI as a layered intrusion that solidified from the sides, inwards, and from the bottom, upwards. However, he could not explain the transition from over- to undersaturated syenites and assumed that the parent magma was nordmarkitic in composition and formed by melting and alkali metasomatism of the local granitic basement.

Kempe & Deer (1976) and Pankhurst *et al.* (1976) argued that the KI was derived from an oversaturated quartz trachyte magma. Pankhurst *et al.* (1976) reported $^{87}Sr/^{86}Sr_i$ values of 0·7045 for the undersaturated rocks and 0·7045–0·7095 for the nordmarkites *sensu lato*. This led Kempe & Deer (1976) to suggest that the quartz trachytic magma differentiated from a mantle-derived alkali olivine basaltic melt, and they speculated that lowering of the liquidus in the Ne–Ks–Q–H_2O system by elevated vapour pressure allowed crossing of the thermal barrier.

Pankhurst *et al.* (1976) observed that the whole-rock oxygen isotope compositions of the foyaites ($\delta^{18}O = 3{\cdot}7$–$4{\cdot}3$‰) are lower than those of the nordmarkites *sensu lato* ($\delta^{18}O = 3{\cdot}7$–$5{\cdot}5$‰). These $\delta^{18}O$ values are below purely mantle-derived magma values ($\delta^{18}O = 5{\cdot}7$–$6{\cdot}5$‰) (e.g. Bindeman *et al.*, 2004). To produce the low $\delta^{18}O$ values of the foyaites, Pankhurst *et al.* (1976) suggested that meteoric water entered the system after ~60% fractionation. Neither Kempe & Deer (1976) nor Pankhurst *et al.* (1976), however, were able to explain fully how the melt was driven towards the nepheline syenite minimum, but discussed possible mechanisms of silica loss and suggested vapour transfer of silica or assimilation of basalt as possible mechanisms.

In conflict with the models described above, Brooks & Gill (1982) found that the most magnesian alkali pyroxenes

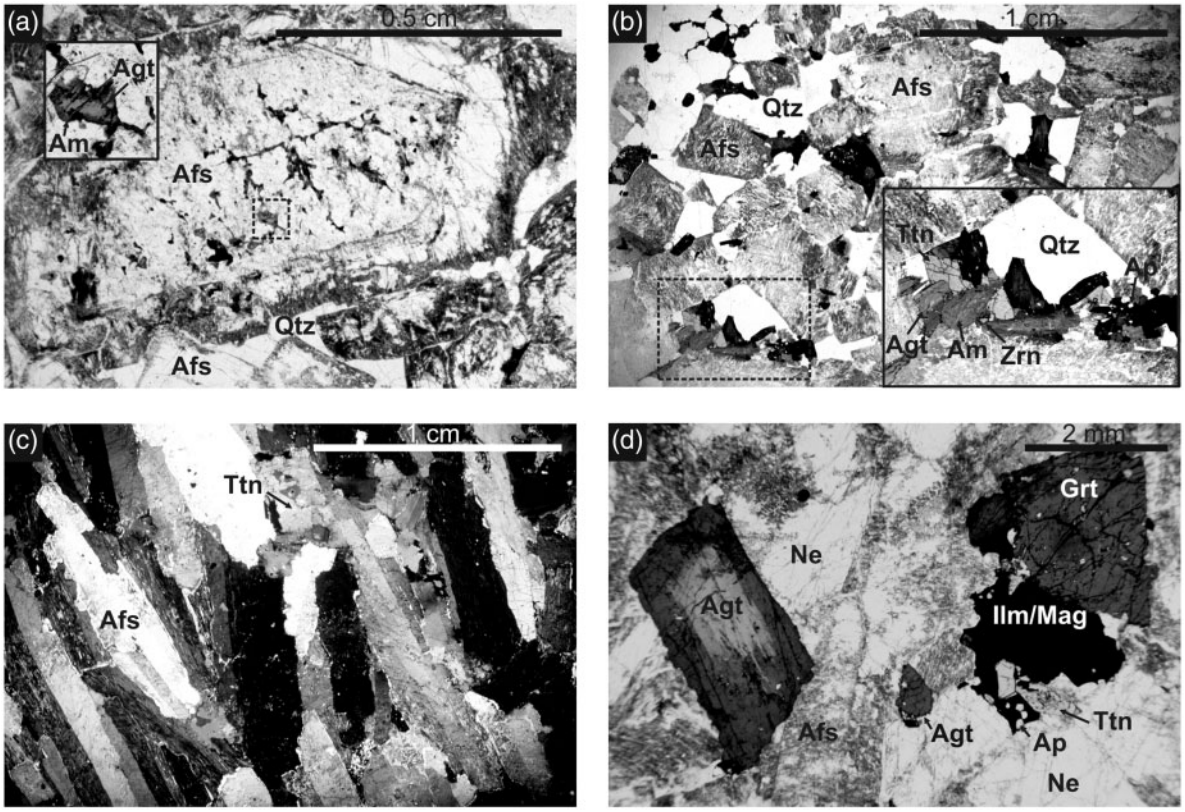

Fig. 3. (a) Zoned alkali feldspar phenocryst in groundmass of finer grained alkali feldspars from quartz nordmarkite (454079) with inclusions of biotite, FeTi-oxides and FeMg-silicates in the central part. The inset (magnification of dashed rectangle) shows an inclusion of aegirine–augite mantled by magnesiokatophorite (plane-polarized light; ppl). (b) Quartz nordmarkite (454079) with euhedral to subhedral alkali feldspar, interstitial quartz and clusters of mafic phases (ppl). The inset shows a typical interstitial cluster of quartz, zoned amphibole (ferrorichterite to arfvedsonite), aegirine–augite, titanite, apatite, zircon and FeTi-oxides. (c) Main pulaskite (454049) displaying igneous lamination defined by parallel arrangement of twinned alkali feldspar laths (cross-polarized light; xpl). (d) Strongly zoned aegirine–augite with irregular shaped core–rim transition and weakly zoned melanite garnet from a foyaite (454050) (ppl). Afs, alkali feldspar; Agt, aegirine–augite; Am, amphibole; Ap, apatite; Grt, garnet; Ilm, ilmenite; Mag, magnetite; Ne, nepheline; Qtz, quartz; Ttn, titanite; Zrn, zircon.

were present in the foyaites and proposed that the foyaites represent the products of fractional crystallization of alkali basalt or nephelinite. In the model of Brooks & Gill (1982), the pulaskites and nordmarkites formed by increasing contamination of the magma with country rock gneiss and basalt. The high $^{87}Sr/^{86}Sr_i$ values of the quartz nordmarkites reported by Pankhurst *et al.* (1976) are consistent with this model and show that the KI did not form as a response to simple closed-system fractional crystallization. Brooks & Gill (1982) pointed to the problem of having enough thermal energy available to heat and assimilate large amounts of wall-rock material, but argued that the crust was probably at an elevated temperature as the Kangerlussuaq area had undergone long-lasting magmatic activity.

FIELD RELATIONS AND SAMPLES

A distinctive feature of the quartz nordmarkites is the presence of trains of huge, elongated, basaltic xenoliths (up to several hundreds of metres across) dipping 30–60° towards the centre of the intrusion (Fig. 2a). A few basaltic xenoliths also occur in the outer parts of the main pulaskites, but otherwise they are absent from the inner part (Wager, 1965). The basaltic xenoliths are fractured and veined by syenite (Fig. 2b). The shape of the contact between basaltic xenoliths and penetrating syenite veins changes from being curved in the marginal part (outer 2–3 cm) of the xenoliths to straight further inwards. When detached in smaller fragments (<20 cm), the xenoliths are rounded and moderately crenulated against a 0–5 cm wide zone of syenite enriched in titanite and FeTi-oxides. Modal layering, defined by the planar concentration of mafic minerals, is locally developed in the quartz nordmarkites (Fig. 2c). Both the nordmarkites and pulaskites locally display igneous lamination defined by platy feldspars (Fig. 3c) dipping 30–60° towards the centre of the intrusion (Wager, 1965). The contact between the KI and the surrounding gneisses dips steeply (70–80°) away from the centre (Wager, 1965). Gneissic xenoliths are rare in the KI.

The alpine topography imposes serious challenges for sampling, as solid syenite outcrops are usually frost-shattered and weathered. Sampling was carried out with helicopter support, which provided an opportunity to retrieve large fresh samples, thereby minimizing the effects of sample heterogeneity. A total of 31 syenite samples were collected from the innermost to outermost part of the KI, together with additional samples of the basaltic xenoliths ($n = 3$), mafic dykes cutting the KI ($n = 3$) and local Archaean basement ($n = 3$). Sample locations are shown in Fig. 1b and global positioning system data are given in Table 1.

Table 1: Major and selected trace elements (XRF) for samples from the Kangerlussuaq Intrusion, East Greenland

Sample	Rock type	Strat. (m)	Sample loc.	Lat. 68N	Long. 32W	SiO_2	TiO_2	Al_2O_3	Fe_2O_3	FeO	MnO	MgO	CaO	Na_2O	K_2O	P_2O_5	LOI	Total
454088	F	0	35	17′17·0″	31′49·4″	55·50	0·51	21·87	1·77	0·83	0·20	0·36	1·84	9·32	6·65	0·11	0·91	98·95
454089	F	0	35	–	–	55·35	0·54	21·69	1·76	0·93	0·19	0·37	1·96	9·34	6·62	0·10	0·84	98·85
454050	F	−500	21	16′47·9″	29′47·9″	56·98	0·26	23·08	1·42	0·65	0·13	0·12	1·05	9·14	7·06	0·03	0·52	99·92
454051	F	−500	21	–	–	57·04	0·26	22·81	1·39	0·64	0·14	0·14	1·19	9·16	7·09	0·03	0·34	99·88
454052	F	−500	21	–	–	56·04	0·24	22·41	1·77	0·40	0·13	0·04	2·07	8·99	7·02	0·04	0·61	99·15
454053	F	−500	21	–	–	57·65	0·18	22·13	1·39	0·43	0·12	0·07	1·62	8·56	7·30	0·03	0·55	99·47
454085	MP	−1000	34	18′08·7″	29′51·9″	63·05	0·62	18·25	1·58	1·52	0·29	0·54	0·55	7·87	5·33	0·05	0·84	99·65
454086	MP	−1000	34	–	–	62·64	0·69	17·89	1·58	1·89	0·22	0·55	0·80	7·05	5·81	0·11	0·95	99·21
454087	MP	−1000	34	–	–	63·61	0·84	17·79	1·07	1·60	0·21	0·67	0·92	7·12	5·96	0·16	0·47	99·93
454047	MP	−1000	20	15′59·7″	27′40·9″	62·72	0·91	17·61	1·82	1·31	0·22	0·76	0·99	7·18	5·89	0·18	0·57	99·59
454048	MP	−1000	20	–	–	63·40	0·91	17·72	1·34	1·34	0·18	0·60	0·86	7·21	6·04	0·16	0·38	99·76
454049	MP	−1000	20	–	–	63·88	0·81	17·81	1·54	0·97	0·17	0·48	0·76	7·19	6·02	0·11	0·46	99·75
454101	MP	−1300	40	19′53·7″	34′55·7″	64·64	0·62	17·99	0·98	1·24	0·11	0·54	0·86	6·96	6·18	0·14	0·24	100·27
454106	TP	−1550	41	18′33·3″	23′57·1″	64·20	0·73	17·18	1·88	1·34	0·16	0·72	0·69	7·78	5·10	0·20	0·26	99·97
454056	TP	−1750	23	14′51·3″	40′51·3″	64·99	0·72	17·17	1·46	1·29	0·17	0·56	0·76	7·80	5·03	0·10	0·16	100·06
454058	TP	−1750	23	–	–	64·10	0·56	17·43	1·56	1·32	0·19	0·59	0·76	7·90	4·96	0·10	0·32	99·47
454110	TP	−1750	43	16′29·1″	22′46·5″	64·06	0·55	17·62	1·35	1·21	0·13	0·52	0·62	7·71	5·30	0·11	0·39	99·18
454097	N	−2300	37	14′11·2″	23′56·6″	65·25	0·72	17·66	1·07	1·22	0·08	0·43	0·61	7·37	5·46	0·07	0·23	99·94
454095A	N	−2800	36	14′17·6″	22′34·0″	67·09	0·77	14·97	2·36	1·38	0·23	0·61	0·49	6·79	4·88	0·12	0·12	99·67
454095B	N	−2800	36	–	–	67·51	0·77	14·62	2·41	1·35	0·22	0·53	0·41	6·66	4·91	0·10	0·11	99·48
454096	N	−2800	36	–	–	65·07	0·95	15·19	2·54	1·58	0·28	0·70	0·64	7·10	4·90	0·15	0·16	99·09
454061	N	−4000	24	14′40·4″	46′28·9″	67·82	0·62	15·00	1·69	1·48	0·19	0·38	0·67	6·48	5·06	0·07	0·23	99·46
454062	N	−4000	24	–	–	65·56	0·78	15·22	1·91	1·92	0·22	0·66	1·26	6·74	4·61	0·16	0·23	99·02
454063	N	−4000	24	–	–	65·47	0·82	14·91	2·10	1·95	0·23	0·66	1·23	6·58	4·71	0·17	0·19	98·83
454111	QN	−5500	39	23′30·5″	40′57·9″	69·25	0·25	13·31	2·63	1·81	0·23	0·39	0·61	6·19	4·94	0·07	0·46	99·68
454078	QN	−6800	32	20′55·4″	57′23·8″	67·64	0·58	14·93	1·94	1·74	0·20	0·44	0·38	6·95	5·26	0·06	0·18	100·12
454079	QN	−6800	32	–	–	70·71	0·57	13·33	1·72	1·55	0·18	0·40	0·55	6·10	4·54	0·08	0·18	99·74
454099	QN	−7000	38	24′23·0″	32′46·1″	66·32	0·91	14·91	1·23	2·98	0·24	0·72	1·13	6·63	4·36	0·20	0·18	99·63
454067	QN	−7500	25	08′23·4″	41′09·9″	66·29	0·80	15·26	1·56	2·38	0·23	0·65	1·07	6·75	4·43	0·18	0·08	99·59
454068	QN	−7500	25	–	–	66·07	0·85	15·24	1·55	2·59	0·24	0·69	1·09	6·77	4·36	0·19	0·04	99·62
454071	QN	−7500	27	08′57·2″	32′34·5″	64·85	0·92	15·86	2·00	2·19	0·23	0·74	1·32	7·01	4·25	0·23	0·16	99·60
454080	BX		32	20′55·4″	57′23·8″	49·26	3·21	13·51	5·61	7·99	0·19	5·61	8·62	4·44	0·99	0·40	0·16	99·82
454081	BX		32	–	–	48·31	3·51	10·66	4·09	9·85	0·20	8·11	10·35	3·30	0·97	0·39	0·38	99·76
454094	BX		36	14′17·6″	22′34·0″	46·87	2·03	14·63	3·41	5·51	0·17	5·56	8·73	4·69	1·94	0·86	4·57	94·41
454090	MD		35	17′17·0″	31′49·4″	45·13	2·60	15·68	4·93	5·04	0·17	5·01	8·59	4·14	2·00	0·76	4·70	94·05
454091	MD		35	–	–	45·23	2·56	13·91	4·67	6·01	0·18	6·38	9·30	3·48	1·48	0·47	5·40	93·69
454098	MD		36	14′17·6″	22′34·0″	44·51	3·03	12·03	3·60	8·09	0·19	8·35	10·07	3·10	1·66	0·47	3·26	95·12
454073	BG		28	08′18·5″	42′48·4″	74·26	0·14	14·48	0·53	0·64	0·03	0·34	2·33	4·21	2·65	0·01	0·34	99·63
454074	BM		28	–	–	60·28	0·65	19·27	1·49	3·51	0·09	2·51	6·55	5·05	0·68	0·12	0·24	100·19
454075	BG		29	10′31·9″	56′45·5″	67·47	0·46	16·12	1·48	2·28	0·05	1·52	4·76	4·35	0·95	0·13	0·30	99·58

(continued)

Table 1: Continued

Sample	PI	V	Cr	Ni	Cu	Zn	Rb	Sr	Y	Zr	Nb	Ba	La	Ce	Pb
454088	1·03	41	b.d.	3	5	88	108	780	23·3	378	115	681	173	267	17
454089	1·04	42	b.d.	3	6	82	104	852	18·9	433	117	741	132	193	16
454050	0·98	23	b.d.	2	2	48	102	146	11·1	254	85	28	124	223	8
454051	1·00	22	b.d.	3	3	46	102	157	13·3	215	76	32	135	236	8
454052	1·00	55	2	3	4	30	103	588	56·8	305	34	104	77	136	8
454053	0·99	42	4	2	3	31	106	626	40·8	300	34	98	73	125	9
454085	1·03	25	b.d.	3	4	158	89	64	15·5	705	230	40	62	115	10
454086	1·00	41	b.d.	2	1	100	69	58	21·6	200	74	167	89	162	6
454087	1·02	29	b.d.	3	3	79	81	99	35·8	151	93	304	135	259	4
454047	1·03	35	b.d.	3	3	104	63	53	34·8	220	88	130	127	245	7
454048	1·04	28	b.d.	3	3	87	63	35	33·6	239	87	94	108	209	8
454049	1·03	26	b.d.	3	2	83	59	32	28·2	249	80	20	98	180	7
454101	1·01	24	b.d.	2	3	56	54	115	15·4	108	39	250	58	104	7
454106	1·07	24	b.d.	3	3	78	62	241	32·1	187	53	1712	88	157	6
454056	1·06	18	b.d.	3	3	79	72	301	34·6	371	102	1275	101	185	9
454058	1·05	17	b.d.	4	4	103	114	326	58·8	674	103	1399	125	222	11
454110	1·05	20	b.d.	4	2	86	100	196	31·0	659	99	1462	88	161	11
454097	1·02	13	b.d.	4	3	73	70	142	60·4	247	91	561	179	343	7
454095A	1·10	5	b.d.	2	2	137	90	28	48·6	395	100	469	133	248	9
454095B	1·11	6	b.d.	2	2	127	91	11	38·1	317	88	144	113	208	6
454096	1·12	5	b.d.	2	4	185	102	52	77·5	776	164	883	182	326	12
454061	1·08	12	b.d.	4	5	188	156	138	82·6	1222	239	346	194	359	15
454062	1·06	26	b.d.	6	4	211	140	407	97·7	1537	242	756	175	326	14
454063	1·07	26	b.d.	5	6	191	150	323	101·9	1648	268	631	199	374	14
454111	1·17	5	b.d.	4	5	255	182	173	75·6	1011	184	472	136	250	21
454078	1·15	8	3	4	3	132	107	16	40·1	481	126	72	70	134	11
454079	1·12	9	b.d.	3	3	118	84	130	35·0	383	103	640	83	155	9
454099	1·05	11	b.d.	4	4	165	86	155	48·5	701	133	1463	100	185	8
454067	1·04	12	b.d.	3	6	154	85	158	46·7	523	118	1612	95	176	11
454068	1·04	11	b.d.	4	5	157	85	166	50·2	617	122	1653	91	168	10
454071	1·02	17	b.d.	3	5	149	69	224	43·9	458	110	1919	75	138	8
454080		336	35	65	130	117	21	549	27·4	255	29	370	42	78	6
454081		360	400	145	120	144	19	568	24·9	254	36	361	42	78	7
454094		262	111	54	80	110	41	1308	22·5	241	86	1309	92	166	21
454090		253	34	45	95	80	36	1684	28·1	257	57	1433	67	118	12
454091		291	173	116	145	86	22	1390	27·1	205	45	1201	56	106	9
454098		308	385	155	65	78	40	573	26·4	286	50	386	44	91	4
454073		11	7	3	12	24	55	192	9·8	82	3	828	25	48	10
454074		86	18	24	10	68	13	273	17·4	95	6	214	18	36	7
454075		41	21	15	5	59	29	264	7·5	140	6	260	29	53	8

F, foyaite; MP, main pulaskite; TP, transitional pulaskite; N, nordmarkite; QN, quartz nordmarkite; BX, basaltic xenolith; MD, mafic dyke; BG, local basement gneiss; BM, basement metabasite; Strat, stratigraphic height; Sample loc., sample location (see Fig. 1b); Lat., latitude (all locations start with 68°N); Long., longitude (all locations start with 32°W); LOI, loss on ignition; PI, peralkalinity index [molar $(Na_2O + K_2O)/Al_2O_3$]; b.d., below detection limit.

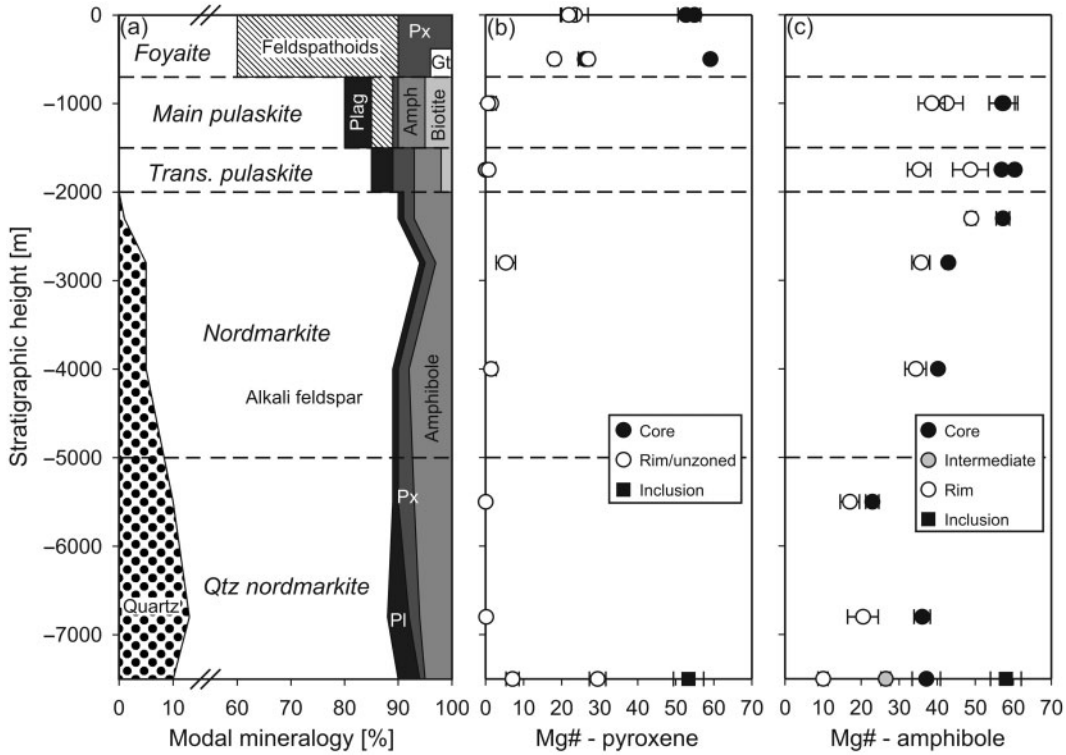

Fig. 4. (a) Modal mineralogy based on visual estimates, (b) pyroxene Mg-number and (c) amphibole Mg-number vs stratigraphic height in the Kangerlussuaq Intrusion. ■, analyses of pyroxene and amphibole inclusions in an alkali feldspar phenocryst from a quartz nordmarkite (454079). Mineral analyses represent means for each sample; horizontal error bars are ±1 SD (±1σ), Pl, plagioclase; Px, pyroxene; Gt, garnet.

STRUCTURE AND STRATIGRAPHY

To present the compositional variations within the intrusion in a simple, stratigraphically meaningful manner, the KI samples have been projected onto a schematic stratigraphic section through the centre of the intrusion. The asymmetric, saucer-shaped structure (Fig. 1c) and the relative radial position of sample locations between the centre and margin of the intrusion (Fig. 1b), taking the petrographic transitions into account, have been used for the projection. The central-most foyaite samples (454088–89) are set to 0 m stratigraphic height, the base of the stratigraphic section (gneiss–quartz nordmarkite contact) is set to −7500 m, and the petrographic transitions foyaite–main pulaskite, main pulaskite–transitional pulaskite, transitional pulaskite–nordmarkite, and nordmarkite–quartz nordmarkite are set to −700 m, −1500 m, −2000 m, and −5000 m, respectively. As an example, main pulaskite sample 454048 is located about two-thirds of the distance from the transitional–main pulaskite transition towards the main pulaskite–foyaite transition (location 20, Fig. 1b), which equals a stratigraphic level of roughly −1000 m.

CLASSIFICATION AND PETROGRAPHY

A summary of petrographic observations (this study; Kempe & Deer, 1970; Kempe *et al.*, 1970) is presented below and a stratigraphic section summarizes the approximate modal variations (Fig. 4a). Except for two samples, they are all peralkaline with peralkalinity indexes [PI, $(Na_2O + K_2O)/Al_2O_3$, molar ratio] of 0·98–1·17 (Table 1).

Quartz nordmarkites

The quartz nordmarkites are classified as quartz alkali feldspar syenites after IUGS (Le Bas & Streckeisen, 1991). They are generally porphyritic, white–yellow to light brown rocks with 0·5–3·0 cm phenocrysts of zoned grey, euhedral, fine microperthitic alkali feldspar laths (Fig. 3a) in a medium-grained groundmass of sub- to anhedral coarse microperthitic alkali feldspars (75–80% total feldspar) and interstitial quartz (10–13%) in clusters with sodic–calcic amphiboles (5–7%), aegirine–augite (1–3%) and accessory magnetite, ilmenite, titanite, apatite, euhedral zircon and chevkinite (Fig. 3b). Albitic rims on groundmass and phenocryst alkali feldspars are common in all rock types of the intrusion. Corona textures with

aegirine–augite rimmed by amphibole are common, with varying core–rim proportions and a 'disintegrated' appearance to the aegirine–augite suggesting replacement. The amphiboles are commonly zoned from light green–brown ferrorichterite in the core to darker green–brown arfvedsonite at the margin (Fig. 3b). Rings of minute inclusions outline the zoning pattern in the alkali feldspar phenocrysts; these include biotite, magnetite, ilmenite and magnesiokatophorite-mantled aegirine–augite in the central parts (Fig. 3a).

Nordmarkites

The nordmarkites are classified as (quartz) alkali feldspar syenites after IUGS (Le Bas & Streckeisen, 1991). These rocks are medium-grained and porphyritic with 0·5–3·0 cm phenocrysts of zoned dark grey, euhedral to subhedral, fine microperthitic alkali feldspar laths in a groundmass of sub- to anhedral microperthitic feldspars (85–90% total feldspar), interstitial quartz (1–5%), commonly zoned sodic–calcic to sodic amphiboles (3–8%), and green pleochroic aegirine–augite (~2%). Accessories are magnetite, ilmenite, plagioclase, biotite, titanite (in one sample up to 3%), apatite, and euhedral zircon. The mafic silicates occur in interstitial clusters with quartz and accessory phases. The alkali feldspar phenocrysts host a variety of inclusions, as in the quartz nordmarkites.

Transitional pulaskites

The transitional pulaskites are coarse-grained inequigranular alkali feldspar syenites with neither quartz nor nepheline. They occasionally contain 1·0–2·5 cm euhedral, fine microperthitic alkali feldspar phenocrysts in a groundmass of euhedral to anhedral coarse microperthitic alkali feldspar (85%), interstitial albitic plagioclase (5%), sodic–calcic to sodic amphiboles (2–7%), aegirine–augite (3–5%) and biotite (~3%). The mafic silicates occur in clusters with accessory titanite, magnetite, ilmenite, and apatite. A variety of amphiboles are present, from unzoned magnesiokatophorite, richterite and ferrorichterite to zoned varieties with magnesiokatophorite (core) to ferrorichterite (rim) and richterite (core) to magnesioarfvedsonite (rim).

Main pulaskites

These coarse-grained grey, foid-bearing alkali feldspar syenites consist of euhedral to anhedral coarse microperthitic feldspars (75–80%), interstitial, zoned amphibole with a light green–yellow magnesiokatophorite (core) to brownish green–yellow katophorite (rim) (5–8%), biotite (4–5%), light green aegirine–augite (1–2%), and euhedral titanite (up to 3–4 mm). Aegirine–augite is present both as an interstitial phase and as inclusions in feldspars. Clusters of interstitial phases include mafic silicates, magnetite, titanite, apatite and occasional melanite garnet. An intergrowth of sodalite, nepheline and cancrinite occurs in interstitial pockets separate from the other interstitial phases. There is no sign of replacement of pyroxene by amphibole, but biotite appears to replace katophorite. Some samples show a distinct igneous lamination defined by oriented alkali feldspar laths (Fig. 3c).

Foyaites

These nepheline syenites have PI of 0·98–1·04 (Table 1) indicating that they are not agpaitic (PI ≥1·2), but miaskitic (PI <1) to intermediate. They are medium-grained inequigranular grey rocks with ~0·5–1·0 cm euhedral to subhedral, coarse microperthitic alkali feldspar (60%) with many minute inclusions, euhedral to subhedral nepheline (25–30%), sodalite (0–8%), aegirine–augite (5–10%) and melanite garnet (0–4%). The aegirine–augite is commonly strongly zoned; the core is weakly pleochroic light yellow to light green, whereas the rim is strongly pleochroic from yellow–green to dark green (Fig. 3d). Although the transition from core to rim is very sharp, the shape of the core is commonly irregular and patchy (Fig. 3d). The mafic phases occur in interstitial clusters and are commonly associated with the feldspathoid minerals (Fig. 3d). The foyaites contain no amphibole. When present, orange–brown subhedral to anhedral melanite garnet occasionally shows colour zoning (Fig. 3d). Sodalite is present as an intergrowth with haüyne, analcite and magnetite.

Basaltic xenoliths

The xenoliths vary texturally from aphyric to pyroxene glomeroporphyritic. The main constituents are plagioclase (50–70%), FeTi-oxides (10–30%), biotite (5–20%), ortho- and clinopyroxene (0–15%), chlorite (0–5%) and carbonate (0–5%). Former vesicles are filled with carbonate. These xenoliths are classified according to the total alkali–silica (TAS) diagram of Le Maitre (2005) as basalts to trachybasalts.

Dykes

The mafic dykes vary from aphyric to plagioclase microporphyritic and pyroxene glomeroporphyritic. The main constituents are plagioclase (45–60%), FeTi-oxide (10–20%), biotite (5–20%), augite (0–30%), sericite (0–15%), chlorite (0–5%) and carbonate (0–5%). Carbonate fills vesicular cavities. Based on the TAS classification scheme, they are trachybasalts.

ANALYTICAL METHODS

A total of 40 whole-rock samples (Table 1) were analysed for major and trace elements by X-ray fluorescence (XRF) on glass discs and pressed powder pellets, respectively, using a Phillips PW-2400 spectrometer at the Department of Earth Sciences, University of Aarhus.

Table 2: Selected average electron microprobe analyses of pyroxenes from the Kangerlussuaq Intrusion, East Greenland

Sample:	454089	454089	454052	454052	454050	454050	454047	454110	454096	454062	454111	454079	454067	454067	454067
Rock type:	F	F	F	F	F	F	MP	TP	N	N	QN	QN	QN	QN	QN
Mineral:	Agt	Agt	Agt	Agt	Agt	Agt	Agt	Agt	Agt	Agt	Agt	Agt	Agt	Agt	Aug
Target:	core	rim	core	rim	core	rim	incl.								
Strat. (m):	0	0	−500	−500	−500	−500	−1000	−1750	−2800	−4000	−5500	−6800	−7500	−7500	−7500
n:	12	11	9	10	9	8	6	9	9	9	9	9	3	6	9
SiO_2	48·75	50·29	49·34	49·62	50·05	49·30	52·46	52·25	50·81	51·24	51·65	51·76	50·08	50·41	51·22
TiO_2	0·93	0·33	0·38	0·32	0·78	0·34	0·53	0·77	0·51	0·22	0·69	3·12	0·29	0·22	0·27
Al_2O_3	3·41	1·27	1·87	1·40	2·53	1·75	0·94	1·05	0·25	0·20	0·24	0·23	0·25	0·20	0·42
FeOT	13·40	19·82	19·41	21·17	11·88	19·46	25·52	26·53	26·05	27·41	29·07	26·26	25·73	20·25	13·94
MnO	1·36	2·96	2·79	3·11	1·45	2·89	0·69	0·44	1·34	0·94	0·60	0·78	1·41	1·78	1·63
MgO	8·36	3·42	4·03	2·62	9·62	3·86	0·22	0·11	0·82	0·23	0·00	0·02	1·11	4·74	8·95
CaO	21·51	15·14	18·39	16·45	22·05	18·13	3·17	3·77	7·69	7·45	2·80	3·27	11·68	17·53	20·86
Na_2O	1·58	4·95	3·15	4·13	1·43	3·22	11·84	11·28	8·60	8·96	11·51	11·44	6·33	3·14	1·51
Total	99·29	98·17	99·37	98·82	99·79	98·95	95·36	96·19	96·07	96·65	96·57	96·88	96·87	98·27	98·81
Fe_2O_3	6·05	12·03	9·15	10·65	5·34	9·06	24·84	23·46	19·31	20·42	26·96	21·78	14·76	7·81	4·22
FeO	7·95	9·00	11·18	11·59	7·07	11·31	3·16	5·41	8·67	9·04	4·81	6·66	12·45	13·23	10·14
New total	99·91	99·38	100·29	99·89	100·33	99·87	97·86	98·55	98·01	98·70	99·28	99·07	98·36	99·06	99·24
Formula based on: 6 oxygen atoms															
Si	1·868	1·972	1·930	1·958	1·897	1·938	2·046	2·035	2·021	2·028	2·014	2·016	2·009	1·993	1·978
Ti	0·027	0·010	0·011	0·009	0·022	0·010	0·016	0·022	0·015	0·007	0·020	0·091	0·009	0·006	0·008
Al	0·154	0·059	0·086	0·065	0·113	0·081	0·043	0·048	0·012	0·009	0·011	0·010	0·012	0·009	0·019
Fe^{3+}	0·174	0·355	0·269	0·316	0·152	0·268	0·729	0·688	0·578	0·608	0·791	0·638	0·445	0·232	0·123
Fe^{2+}	0·255	0·295	0·366	0·382	0·224	0·372	0·103	0·176	0·289	0·299	0·157	0·217	0·418	0·437	0·328
Mn	0·044	0·098	0·092	0·104	0·047	0·096	0·023	0·015	0·045	0·032	0·020	0·026	0·048	0·060	0·053
Mg	0·477	0·200	0·235	0·154	0·544	0·226	0·013	0·007	0·049	0·013	0·000	0·001	0·066	0·280	0·515
Ca	0·883	0·636	0·771	0·695	0·896	0·764	0·132	0·157	0·328	0·316	0·117	0·138	0·502	0·742	0·863
Na	0·118	0·376	0·239	0·316	0·105	0·245	0·895	0·851	0·663	0·687	0·870	0·862	0·492	0·240	0·113
Total	4·000	4·000	4·000	4·000	4·000	4·000	4·000	4·000	4·000	4·000	4·000	4·000	4·000	4·000	4·000
En	24·5	10·2	11·9	7·8	27·6	11·5	0·7	0·3	2·5	0·7	0·0	0·1	3·4	14·0	25·8
Fs	24·3	38·2	36·9	40·8	21·5	37·3	45·1	46·4	46·7	48·0	49·5	46·8	46·2	36·6	25·2
Wo	45·3	32·5	39·1	35·3	45·5	38·7	7·0	8·3	16·8	16·2	6·0	7·3	25·5	37·3	43·3
Ac	6·0	19·2	12·1	16·0	5·3	12·4	47·2	45·0	34·0	35·1	44·5	45·8	25·0	12·1	5·7
Mg-no.	52·7	23·5	27·0	18·1	59·1	26·1	1·5	0·8	5·3	1·5	0·0	0·1	7·1	29·5	53·4

F, foyaite; MP, main pulaskite; TP, transitional pulaskite; N, nordmarkite; QN, quartz nordmarkite; Agt, aegirine–augite; Aug, sodian augite; Strat., stratigraphic height; Mg-number $= 100 \times Mg/(Mg + Fe^{2+}(total))$; *n*, number of analyses (three points in each of several grains). Ferric iron concentrations have been calculated using equation (3) of Droop (1987).

Altered surfaces were removed prior to whole-rock powder preparation.

Mineral compositions were determined with a JEOL JXA-8600 Superprobe at the Department of Earth Sciences, University of Aarhus, using a beam current of 15 nA, accelerating voltage of 15 kV and 5 μm beam diameter. Pyroxenes were analysed for Al, Ti, Cr, Mn, Ca and Na (wavelength-dispersive spectrometry; WDS), and Si, Fe and Mg (energy-dispersive spectrometry; EDS). Amphiboles were analysed for Cr, Mn, Ca, Na and K (WDS), and Si, Al, Ti, Fe and Mg (EDS). Counting times for WDS were 40 s or until the standard deviation on total counts was less than 1%. Counting times for EDS were 200 s. The mineral chemistry was commonly based on three analysis points in each of several grains. Data given in Tables 2 and 3 represent average compositions of pyroxenes and amphiboles, respectively.

Titanite ($n = 7$) and alkali feldspar ($n = 12$) minor and trace element analyses were carried out by inductively coupled plasma mass spectrometry (ICP-MS) at

Table 3: Selected average electron microprobe analyses of amphiboles from the Kangerlussuaq Intrusion, East Greenland

Sample:	454047	454047	454110	454110	454097	454097	454062	454062	454111	454111	454079	454079	454067	454067	454067	454067
Rock type:	MP	MP	TP	TP	N	N	N	N	QN	QN	QN	QN	QN	QN	QN	QN
Mineral:	mk	k	r	ma	mk	r	fr	fr	a	a	fr	a	mk	fr	fr	fw
Target:	core	rim	core	rim	core	rim	core	rim	core	rim	core	rim	incl.	core	int/rim	rim
Strat. (m):	−1000	−1000	−1750	−1750	−2300	−2300	−4000	−4000	−5500	−5500	−6800	−6800	−7500	−7500	−7500	−7500
n:	7	5	2	7	8	4	3	7	9	7	4	3	5	6	12	3
SiO_2	48·68	47·71	51·20	49·36	49·29	50·60	50·54	49·82	50·69	50·33	50·60	50·06	49·64	49·30	48·63	49·39
TiO_2	1·59	1·58	1·13	1·43	1·29	0·87	0·82	1·00	0·95	1·21	1·32	1·69	0·55	1·05	1·16	0·20
Al_2O_3	3·83	3·99	2·30	3·39	3·01	1·43	1·67	1·60	0·74	0·60	0·81	0·41	2·69	1·50	1·38	0·72
FeOT	15·40	19·78	15·65	17·91	15·80	18·85	21·68	23·23	25·35	26·94	21·83	26·02	15·66	22·27	25·68	32·26
MnO	1·93	2·22	1·92	1·86	1·54	1·84	2·11	2·14	2·07	2·18	1·98	2·27	1·44	1·70	1·76	1·18
MgO	11·47	8·20	11·58	9·58	11·88	10·14	8·17	6·82	4·24	3·12	6·92	3·78	12·18	7·40	5·18	2·01
CaO	5·49	3·91	3·24	2·80	6·74	5·62	4·93	4·71	0·99	0·89	3·54	2·04	7·87	6·08	5·13	4·73
Na_2O	6·46	7·21	7·70	7·86	5·13	5·32	5·99	5·99	8·49	8·32	7·20	7·76	4·42	4·94	5·24	4·37
K_2O	1·38	1·38	1·33	1·42	1·15	1·15	1·15	1·15	1·38	1·42	1·26	1·36	1·15	1·06	1·08	0·71
Total	96·24	95·97	96·05	95·60	95·83	95·83	97·05	96·46	94·90	95·02	95·46	95·38	95·60	95·31	95·24	95·58
Fe_2O_3	2·66	4·01	4·07	4·31	3·24	4·42	4·23	4·07	1·91	2·03	0·10	0·68	2·22	2·29	3·63	7·62
FeO	13·00	16·17	11·98	14·03	12·88	14·87	17·87	19·57	23·62	25·11	21·74	25·41	13·67	20·21	22·42	25·40
New total	96·50	96·37	96·46	96·05	96·16	96·28	97·48	96·87	95·10	95·22	95·47	95·45	95·83	95·54	95·60	96·34
Formula based on 23 oxygen atoms and assuming a total of 13 cations exclusive of Ca, Na and K																
Si	7·358	7·362	7·674	7·525	7·448	7·704	7·710	7·721	8·080	8·080	7·945	8·022	7·529	7·726	7·727	7·892
Al^{IV}	0·642	0·638	0·326	0·475	0·536	0·257	0·290	0·279	0·000	0·000	0·055	0·000	0·471	0·274	0·258	0·108
Sum T	8·000	8·000	8·000	8·000	7·983	7·961	8·000	8·000	8·080	8·080	8·000	8·022	8·000	8·000	7·985	8·000
Al^{VI}	0·041	0·087	0·080	0·135	0·000	0·000	0·010	0·014	0·140	0·114	0·094	0·078	0·011	0·003	0·000	0·027
Ti	0·181	0·183	0·128	0·164	0·147	0·100	0·094	0·117	0·114	0·146	0·156	0·203	0·063	0·124	0·138	0·024
Fe^{3+}	0·302	0·466	0·459	0·495	0·368	0·506	0·486	0·473	0·230	0·245	0·012	0·082	0·253	0·269	0·433	0·916
Mg	2·586	1·887	2·588	2·176	2·676	2·301	1·858	1·577	1·007	0·745	1·619	0·902	2·753	1·728	1·227	0·479
Fe^{2+}	1·643	2·087	1·502	1·790	1·628	1·894	2·279	2·538	3·149	3·373	2·856	3·405	1·734	2·651	2·979	3·394
Mn	0·247	0·290	0·243	0·240	0·181	0·199	0·272	0·280	0·280	0·297	0·263	0·308	0·185	0·226	0·222	0·160
Sum C	5·000	5·000	5·000	4·998	5·000	5·000	5·000	4·999	4·919	4·920	5·000	4·978	4·999	5·000	5·000	5·000
Mn	0·000	0·000	0·000	0·000	0·016	0·038	0·000	0·000	0·000	0·000	0·000	0·000	0·000	0·000	0·015	0·000
Ca	0·890	0·647	0·520	0·459	1·092	0·918	0·806	0·784	0·169	0·154	0·595	0·350	1·280	1·022	0·874	0·812
Na	1·109	1·353	1·480	1·541	0·891	1·044	1·194	1·216	1·831	1·846	1·405	1·650	0·720	0·978	1·111	1·188
Sum B	2·000	2·000	2·000	2·000	2·000	2·000	2·000	2·000	2·000	2·000	2·000	2·000	2·000	2·000	2·000	2·000
Na	0·786	0·808	0·763	0·788	0·614	0·530	0·583	0·587	0·795	0·746	0·789	0·762	0·581	0·524	0·504	0·169
K	0·266	0·271	0·255	0·277	0·222	0·225	0·223	0·228	0·281	0·291	0·253	0·278	0·223	0·212	0·219	0·146
Sum A	1·052	1·079	1·017	1·065	0·836	0·755	0·806	0·815	1·076	1·037	1·042	1·041	0·804	0·736	0·724	0·315
Total	16·052	16·079	16·017	16·063	15·819	15·716	15·806	15·814	16·075	16·037	16·042	16·040	15·803	15·736	15·709	15·315
Mg-no.	57·1	42·5	56·9	48·7	57·3	49·0	40·2	34·4	23·0	17·1	36·1	20·5	58·1	37·2	26·5	10·0

F, foyaite; MP, main pulaskite; TP, transitional pulaskite; N, nordmarkite; QN, quartz nordmarkite; mk, magnesiokatophorite; k, katophorite; r, richterite; fr, ferrorichterite; ma, magnesioarfvedsonite; a, arfvedsonite; fw, ferrowinchite; Strat., stratigraphic height; Mg-number $= 100 \times Mg/(Mg + Fe^{2+}(total))$; *n*, number of analyses (three points in each of several grains). Ferric iron concentrations have been calculated using equation (6) of Droop (1987). The amphibole nomenclature is after Leake *et al*. (1997).

Geocenter Copenhagen using a Perkin Elmer Sciex system equipped with a 266 nm Nd–YAG laser ablation facility (Tables 4 and 5). The phases were targeted *in situ* using slabs from thin-section preparations. The laser was operated at beam sizes of 100 μm (external glass standard NIST SRM 610; Pearce *et al.*, 1997) and 200 μm (samples). ^{30}Si was used as internal standard for both titanites and alkali feldspars using known concentrations from

Table 4: Trace element analyses (LA-ICP-MS) of titanites from the Kangerlussuaq Intrusion, East Greenland

Sample	Rock type	Strat. (m)	*n*	Y	Zr	Nb	La	Ce	Pr	Nd	Sm	Eu	Gd	Dy	Er	Yb	Hf	Ta
454088	F	0	15	537	4935	6601	3441	5528	513	1426	160	46	131	98	52	40	129	138
454089	F	0	8	723	3569	5602	3292	6041	722	2309	294	79	209	151	67	49	99	224
454050	F	−500	18	941	5294	6489	3852	8017	979	3436	450	82	318	209	91	61	166	398
454048	MP	−1000	46	1430	1928	2888	3666	7915	1252	5723	932	245	640	370	132	81	63	259
454110	TP	−1750	16	1856	2982	5590	4188	8548	1273	5319	977	251	708	511	190	102	96	370
454097	N	−2300	42	4241	3513	3984	5247	12953	2829	14460	3218	502	2235	1505	440	218	124	505
454079	QN	−6800	15	2022	884	3509	3428	9253	1840	8842	1799	275	1172	740	210	97	32	340

F, foyaite; MP, main pulaskite; TP, transitional pulaskite; N, nordmarkite; QN, quartz nordmarkite; Strat., stratigraphic height; *n*, number of replicates.

Table 5: Selected trace element analyses (LA-ICP-MS) of alkali feldspars from the Kangerlussuaq Intrusion, East Greenland

Sample	Rock type	Strat. (m)	Phase	*n*	Fe	Rb	Sr	Ba	Pb	Th	U
454089	F	0	undif	30	1875	123	742	773	8·8	1·2	0·5
454050	F	−500	undif	45	1759	107	140	57	8·4	1·0	0·9
454052	F	−500	undif	15	1932	91	454	125	3·4	0·3	0·5
454048	MP	−1000	undif	25	3520	48	23	65	2·6	0·3	0·2
454110	TP	−1750	undif	66	5471	85	116	1139	1·1	0·7	0·3
454097	N	−2300	phx	15	5185	57	64	264	2·4	0·2	0·5
454097	N	−2300	mtx	19	4224	70	40	215	3·9	0·5	0·7
454062	N	−4000	mtx	17	6492	107	52	141	3·6	0·1	0·1
454111	QN	−5500	mtx	13	4648	195	60	396	1·6	0·5	0·3
454079	QN	−6800	mtx	21	10629	108	5	69	2·5	6·0	1·1
454067	QN	−7500	phx	27	4606	21	571	4738	8·7	1·6	0·5
454067	QN	−7500	mtx	22	3583	21	37	355	2·4	0·2	0·2

F, foyaite; MP, main pulaskite; TP, transitional pulaskite; N, nordmarkite; QN, quartz nordmarkite; undif, undifferentiated alkali feldspar (i.e. mixture of several populations; if present)); phx, alkali feldspar phenocryst; mtx, matrix alkali feldspar; Strat., stratigraphic height; *n*, number of replicates.

microprobe analyses. Time-resolved replicate analyses of single crystals were carefully screened for the presence of inclusions (e.g. zircon and apatite) along the line scans. Selected trace and minor elements with standard errors less than 20% for titanite and less than 27% for alkali feldspar are presented. Pb, Th and U concentrations for alkali feldspars are included for purpose of age-correcting the Pb isotope data, although the errors are larger.

Sr–Nd–Hf–Pb isotope analyses were carried out on 19 representative samples at Geocenter Copenhagen (Table 6). Sr isotopes were measured by thermal ionization mass spectrometry (TIMS), and Nd, Hf and Pb isotopes were measured using the VG Elemental Axiom multi-collector (MC)-ICP-MS system at the Danish Lithosphere Centre. Separates of Sr for isotopic analysis were prepared from whole-rock powders by standard ion-exchange procedures. The $^{87}Sr/^{86}Sr$ data were measured in one analytical session and the NBS987 standard gave $^{87}Sr/^{86}Sr = 0{\cdot}710249 \pm 26$ (2 SD, $n = 5$). Whole-rock samples for Sm–Nd and Lu–Hf isotope determinations underwent flux fusion digestion and chemical separation procedures described by Bizzarro *et al.* (2003) and Ulfbeck *et al.* (2003). The Nd and Hf data were acquired in two analytical sessions, in which the Ames metal standard gave $^{143}Nd/^{144}Nd = 0{\cdot}512136 \pm 13$ (25 ppm, 2 SD, $n = 11$) and $0{\cdot}512129 \pm 7$ (13 ppm, 2 SD, $n = 4$), and the DLC Hf

Table 6: Sr–Nd–Hf–Pb isotope data for samples from the Kangerlussuaq Intrusion, East Greenland

Sample whole-rock	Rock type	Strat. (m)	$^{87}Sr/^{86}Sr$ measured	$^{87}Sr/^{86}Sr$ initial	Sm (ppm)	Nd (ppm)	$^{143}Nd/^{144}Nd$ measured	$^{143}Nd/^{144}Nd$ initial	ε_{Nd} initial	Lu (ppm)	Hf (ppm)	$^{176}Hf/^{177}Hf$ measured	$^{176}Hf/^{177}Hf$ initial	ε_{Hf} initial
454089	F	0	0·70469	0·70444	3·86	35·31	0·512791	0·512769	3·8	0·25	8·34	0·283058	0·283054	11·1
454050	F	−500	0·70572	0·70428	3·48	44·44	0·512840	0·512825	4·9	0·18	5·13	0·283050	0·283045	10·8
454052	F	−500	0·70464	0·70428	8·65	57·05	0·512846	0·512816	4·7	1·34	7·08	0·283068	0·283041	10·7
454048	MP	−1000	0·70813	0·70440	21·24	133·73	0·512832	0·512801	4·4	0·27	5·50	0·283043	0·283036	10·5
454110	TP	−1750	0·70552	0·70447	11·04	70·36	0·512769	0·512738	3·2	0·43	15·21	0·282984	0·282980	8·5
454097	N	−2300	0·70556	0·70455	46·49	239·95	0·512779	0·512741	3·3	0·63	6·56	0·282946	0·282932	6·8
454096	N	−2800	0·70900	0·70495	31·35	190·36	0·512770	0·512738	3·2	1·40	20·40	0·282931	0·282921	6·5
454062	N	−4000	0·70547	0·70476	27·70	163·43	0·512785	0·512752	3·5	1·32	38·31	0·282931	0·282926	6·6
454111	QN	−5500	0·70705	0·70489	18·81	113·85	0·512782	0·512749	3·4	1·73	28·42	0·282934	0·282926	6·6
454079	QN	−6800	0·70626	0·70494	12·94	77·80	0·512765	0·512732	3·1	0·69	9·95	0·282922	0·282913	6·1
454067	QN	−7500	0·70717	0·70607	16·02	93·64	0·512726	0·512692	2·3	0·68	15·62	0·282892	0·282886	5·2
454073	BG		0·73559	0·73500	0·59	3·77	0·510895	0·510864	−33·4	0·19	2·42	0·281693	0·281682	−37·4
454074	BM		0·71472	0·71462	3·32	14·13	0·511711	0·511664	−17·7	0·32	2·89	0·281633	0·281617	−39·7
454075	BG		0·72858	0·72836	1·94	11·18	0·511036	0·511001	−30·7	0·12	3·36	0·281162	0·281157	−55·9
454080	BX		0·70561	0·70553	8·73	43·08	0·512533	0·512493	−1·6	0·49	6·54	0·282628	0·282617	−4·3
454081	BX		0·70473	0·70466	8·95	44·78	0·512635	0·512595	0·4	0·26	6·60	0·282754	0·282749	0·3
454091	MD		0·70454	0·70451	8·61	51·31	0·512685	0·512651	1·5	0·30	4·44	0·282923	0·282914	6·2

Sample	$^{206}Pb/^{204}Pb$ measured	$^{207}Pb/^{204}Pb$ measured	$^{208}Pb/^{204}Pb$ measured	$^{206}Pb/^{204}Pb$ initial	$^{207}Pb/^{204}Pb$ initial	$^{208}Pb/^{204}Pb$ initial
alkali feldspar						
454089 undif	17·783	15·350	37·557	17·75	15·35	37·54
454050 undif	17·882	15·369	37·642	17·83	15·37	37·62
454052 undif	17·812	15·359	37·576	17·74	15·36	37·56
454048 undif	17·686	15·331	37·708	17·64	15·33	37·69
454110 undif	17·666	15·292	37·907	17·54	15·29	37·80
454097 phx	17·277	15·247	37·527	17·19	15·24	37·51
454097 mtx	17·338	15·256	37·578	17·25	15·25	37·56
454096 phx	17·145	15·216	37·465			
454096 mtx	17·256	15·227	37·614			
454062 undif	17·206	15·212	37·691	17·19	15·21	37·69
454111 undif	17·254	15·208	37·948	17·17	15·20	37·90
454079 undif	17·268	15·201	37·934	17·05	15·19	37·55
454067 undif	16·977	15·160	37·685	16·95	15·16	37·66
whole-rock						
454073	15·159	14·962	35·061			
454074	20·010	15·888	37·161			
454075	15·106	14·924	37·427			
454080	15·889	15·251	37·142			
454081	16·522	15·011	36·604			
454091	17·071	15·264	36·943			

F, foyaite; MP, main pulaskite; TP, transitional pulaskite; N, nordmarkite; QN, quartz nordmarkite; BX, basaltic xenolith; MD, mafic dyke; BG, local basement gneiss; BM, basement metabasite; undif, undifferentiated alkali feldspar (i.e. mixture of several populations; if present); phx, alkali feldspar phenocryst; mtx, matrix alkali feldspar; Strat., stratigraphic height. Initial magmatic ratios and basement crust ratios calculated back to an age of 50 Ma.

standard gave $^{176}Hf/^{177}Hf = 0{\cdot}281847 \pm 9$ (2 SD, $n = 11$) and $0{\cdot}281852 \pm 11$ (2 SD, $n = 6$). Sr, Nd and Hf ratios are normalized relative to accepted values for NBS987 (0·71025), Ames metal (0·512125) and DLC Hf (0·281890) standards. Pb isotopes were determined on either alkali feldspar separates (syenites), hand-picked 0·5–1·0 mm rock chips (basalts or dykes) or whole-rock powders (basement) that were leached in hot 6M HCl for ~1 h prior to sample digestion and Pb separation. The Pb samples were measured in two analytical sessions, in which the SRM981 standard gave $^{206}Pb/^{204}Pb = 16{\cdot}9402 \pm 17$, $^{207}Pb/^{204}Pb = 15{\cdot}4984 \pm 25$ and $^{208}Pb/^{204}Pb = 36{\cdot}7229 \pm 64$ (2 SD, $n = 2$) and $^{206}Pb/^{204}Pb = 16{\cdot}9404 \pm 2$, $^{207}Pb/^{204}Pb = 15{\cdot}4978 \pm 7$ and $^{208}Pb/^{204}Pb = 36{\cdot}7210 \pm 16$ (2 SD, $n = 2$), using Pb double spike to correct for mass bias following the technique of Baker *et al.* (2004). Initial Sr, Nd, Hf and Pb isotope ratios are calculated back to an age of 50 Ma using the Rb and Sr concentrations measured on glass discs by XRF, Sm, Nd, Lu and Hf concentrations measured by isotope dilution, and Pb, U and Th concentrations measured by ICP-MS and laser ablation (LA)-ICP-MS.

MINERAL CHEMISTRY

Mineral chemical data for pyroxenes and amphiboles are given in Tables 2 and 3. The variation of Mg-number with stratigraphic height in alkali pyroxenes and sodic–calcic to sodic amphiboles is presented in Fig. 4b and c. In the stratigraphically lowest quartz nordmarkites (−7500 m), interstitial aegirine–augite with ferrorichterite rims has Mg-number 29·5, whereas an aegirine–augite without amphibole rim has Mg-number 7·1. Inclusions of pyroxene in alkali feldspar phenocrysts have a much more primitive sodian augite composition with Mg-number 53·4. Interstitial aegirine–augites from the overlying quartz nordmarkites, nordmarkites and pulaskites have magnesium contents below Mg-number 5·3 and typically less than 1·0. Mg-number px increases markedly from the main pulaskites into the foyaites. Aegirine–augite in the foyaites have Mg-numbers of 52·7–59·1 (cores) and 21·9–27.0 (rims). As shown by Brooks & Gill (1982) and in Table 2, the pyroxene cores in the foyaites and pyroxene inclusions in quartz nordmarkite sample 454067 are clearly less acmitic ($En_{24–27}Fs_{21–25}Wo_{43–45}Ac_{5–6}$) than their corresponding rims and interstitial pyroxenes ($En_{0–10}Fs_{37–50}Wo_{6–39}Ac_{12–47}$). Excluding the stratigraphically lowest sample (454067, −7500 m), all pyroxenes in nordmarkites *sensu lato* and transitional pulaskite are relatively sodic and have extremely low Mg contents.

In Fig. 4c we document for the first time systematic variations in amphibole compositions from the KI. From the stratigraphically lowest quartz nordmarkite to the quartz nordmarkites at −5500 m, the core compositions of interstitial amphiboles change from Mg-number 37·2 to 23·0. Stratigraphically upwards from −5500 m, amphibole cores become more magnesian, increasing to Mg-number 56·9–60·4 in the pulaskites. The rim Mg-number of zoned amphiboles is consistently lower than the cores, but mimics the up-section increase in Mg-number of the cores. Amphibole rims (Mg-number 58·1) on aegirine–augite included in alkali feldspar phenocrysts from the stratigraphically lowest quartz nordmarkites are similar in composition to amphiboles in the pulaskites.

WHOLE-ROCK CHEMISTRY

Major elements

Concentrations of SiO_2, Al_2O_3, $Na_2O + K_2O$ and Mg-number from the KI and associated samples from dykes, basaltic xenoliths and local basement gneisses (Table 1) are plotted against stratigraphic height in Fig. 5a–d. SiO_2 first increases from ~65 wt % in the stratigraphically lowest quartz nordmarkites (−7500 m) to ~70 wt % in the quartz nordmarkites at −5500 m, then displays a gradual decrease through the nordmarkites to ~63 wt % in the main pulaskites (Fig. 5a), followed by an abrupt drop into the foyaites (~56 wt %). The Al_2O_3 trend is opposite to that of SiO_2 (Fig. 5b). The total alkalis increase gradually from the quartz nordmarkites (~11 wt %) through the pulaskites (~13 wt %), followed by an abrupt increase into the foyaites (~16 wt %). Whole-rock Mg-number (Fig. 5d) decreases from ~25 in quartz nordmarkites at −7500 m to a low of ~14 at −5500 m, then increases through the nordmarkites and pulaskites to ~30. Whole-rock Mg-number varies from 5 to 20 in the foyaites.

Trace elements

Trace element data for 40 whole-rock samples are presented in Table 1 and Fig. 5e–h. The data generally display large variations for samples from the same inferred stratigraphic height as a result of variable accumulation of accessory phases such as titanite, zircon and chevkinite, but some systematic trends can be recognized. V increases from a fairly constant level of 5–12 ppm in the nordmarkites *sensu lato* to ~40 ppm in the foyaites (Fig. 5e). Zr increases from 400–700 ppm in the quartz nordmarkites to 1200–1650 ppm in the nordmarkites at −4000 m, followed by a decrease through the uppermost nordmarkites to 200–400 ppm in the foyaites (Fig. 5f). Rb also shows a high of 150–170 ppm in the middle part of the silica-oversaturated stratigraphy (−4000 m to −5500 m) and lows of 50–100 ppm below and above. Sr increases from a fairly constant low level of ~200 ppm in the quartz nordmarkites through pulaskites to a high of ~800 ppm in the foyaites (Fig. 5h).

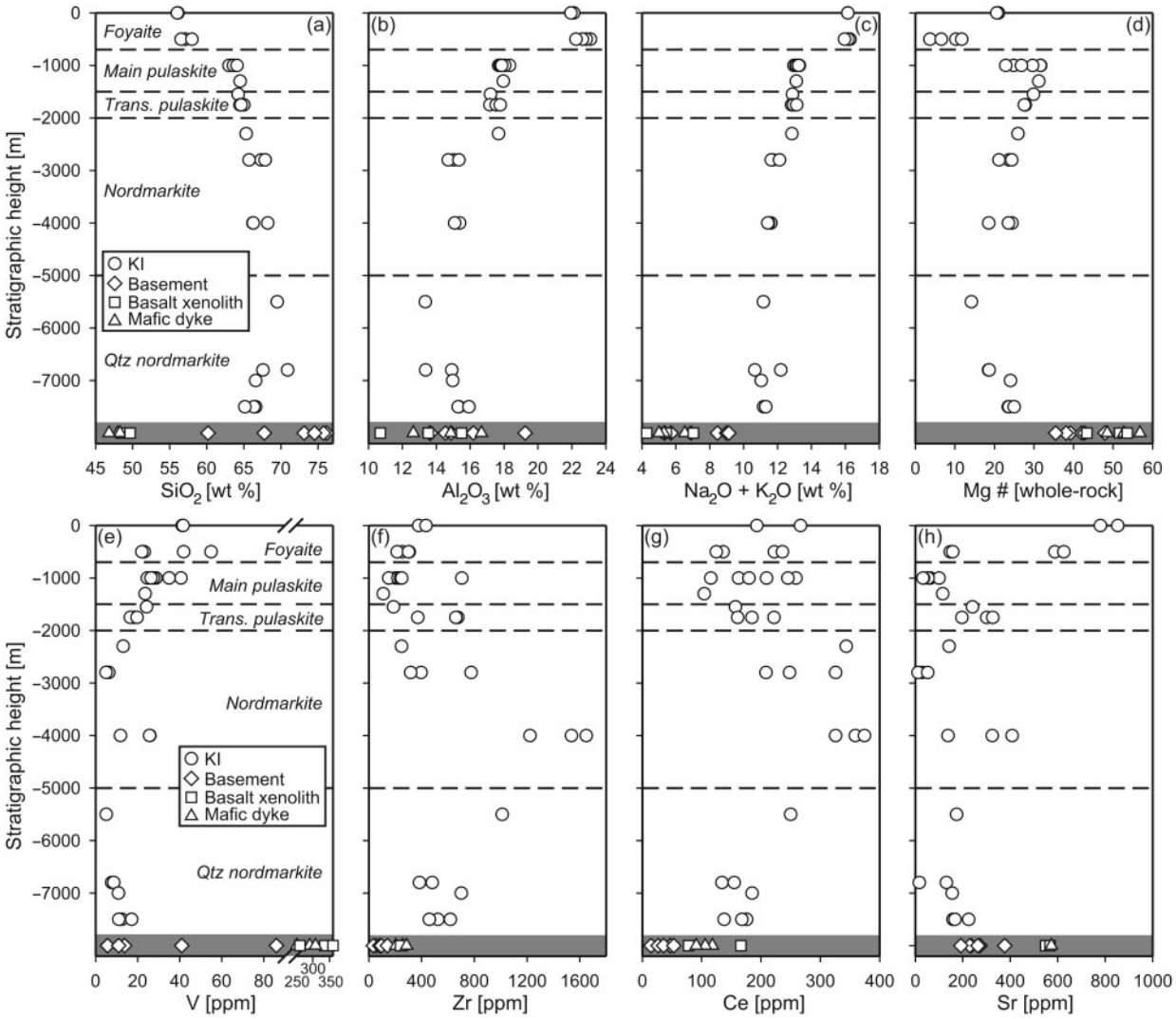

Fig. 5. Selected whole-rock (a–c) major element oxides, (d) Mg-number [$100 \times Mg/(Mg + Fe^{2+}(total))$] and (e–h) trace elements in the Kangerlussuaq Intrusion vs stratigraphic height. Compositions of basement rocks [including data from Riishuus *et al.* (2005)], basaltic xenoliths and dykes are given in the grey band at the base of each plot.

IN SITU TITANITE AND FELDSPAR MINOR AND TRACE ELEMENTS

Titanite

Minor and trace element data from seven samples are given in Table 4. Variations in titanite rare earth element (REE)concentrations are presented in a chondrite-normalized REE diagram (Fig. 6). Titanite can accommodate large quantities of REE and high field strength elements (HFSE) and all the samples are extremely enriched in these elements. REE abundances in titanite increase upwards from the quartz nordmarkites into the nordmarkites followed by a decrease through the uppermost foyaites. Titanites from all samples are enriched in light REE (LREE) compared with heavy REE (HREE). The foyaites show the steepest trends as they have relatively lower HREE. The quartz nordmarkites to main pulaskites have convex-upwards REE patterns, whereas the uppermost foyaites display convex-downwards patterns. The two nordmarkite samples and one foyaite display negative Eu anomalies. The Ta content of titanite increases from ~350 ppm at −7500 m in the quartz nordmarkites to ~500 ppm in the upper nordmarkites, followed by a decrease through the foyaites to 140–220 ppm (Table 4).

Alkali feldspar

Minor and trace element data from 12 feldspar samples are given in Table 5. Fe in matrix alkali feldspars displays

a steady increase from ~3600 ppm in the quartz nordmarkites to ~6500 ppm in the nordmarkites, followed by a sharp decrease through the pulaskites to ~1900 ppm in the foyaites. One quartz nordmarkite outlier has more than 10 000 ppm Fe but also a large standard deviation. The trend of alkali feldspar Fe enrichment or depletion is roughly similar to that of whole-rock SiO_2, Zr and Ce (REE) variation (Fig. 5a, f and g). The Sr concentrations of matrix alkali feldspars principally show the same variation as the whole-rock contents, increasing from a constant low level of ~50 ppm in the quartz nordmarkites through pulaskites to a high of 400–800 ppm in the foyaites (Table 5). Alkali feldspar phenocrysts from a quartz nordmarkite (454067) show much higher Sr concentrations (~600 ppm) than the coexisting matrix feldspar (~50 ppm), and the phenocryst content is similar to that of feldspar in the foyaites. Higher in the nordmarkite stratigraphy the phenocrysts are not significantly different from the matrix. Rb in alkali feldspar varies in a similar way to that in whole-rock (Tables 3 and 5).

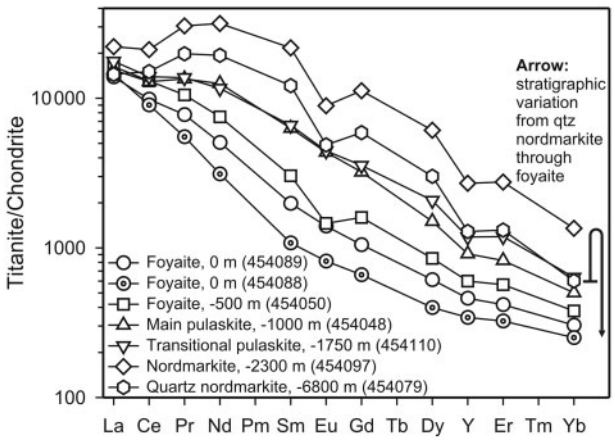

Fig. 6. Chondrite-normalized REE abundance patterns for titanites from the Kangerlussuaq Intrusion. Chondrite normalization values are from McDonough & Sun (1995). The arrow indicates the direction of stratigraphic variations from a quartz nordmarkite (454079, −6800 m) to the uppermost foyaite (454089, 0 m).

Sr–Nd–Hf–Pb ISOTOPES

Sr, Nd, Hf and Pb isotope data on 19 whole-rock and alkali feldspar samples are presented in Table 6. $^{87}Sr/^{86}Sr_i$ (50 Ma) decreases markedly from ~0·706 in the lowermost quartz nordmarkites to ~0·705 at −6800 m, followed by a gradual decrease through the stratigraphy to 0·7043–0·7044 in the foyaites (Fig. 7a). ε_{Ndi} and ε_{Hfi} both increase through the stratigraphy from the lowermost quartz nordmarkites ($\varepsilon_{Ndi} = 2{\cdot}3$, $\varepsilon_{Hfi} = 5{\cdot}2$), over a constant level in the nordmarkites ($\varepsilon_{Ndi} = 3{\cdot}1–3{\cdot}5$, $\varepsilon_{Hfi} = 6{\cdot}5–6{\cdot}6$), to the foyaites ($\varepsilon_{Ndi} = 3{\cdot}8–4{\cdot}9$, $\varepsilon_{Hfi} = 10{\cdot}7–11{\cdot}1$) (Fig. 7b and c). The Archaean basement samples have very radiogenic $^{87}Sr/^{86}Sr_{50\ Ma}$ compositions (0·715–0·735) and very unradiogenic $\varepsilon_{Nd,\ 50\ Ma}$ (−18 to −33) and $\varepsilon_{Hf,\ 50\ Ma}$ (−37 to −56) compositions. The mafic dyke and basaltic xenoliths have $^{87}Sr/^{86}Sr_i$ (50 Ma) = 0·7045–0·7055, $\varepsilon_{Ndi} = 0{\cdot}4–1{\cdot}5$ and $\varepsilon_{Hfi} = -4{\cdot}3$ to 6·2.

The alkali feldspar $^{207}Pb/^{204}Pb_{meas}$–$^{206}Pb/^{204}Pb_{meas}$ variation is shown in Fig. 8. Alkali feldspars have more radiogenic Pb isotopic compositions ($^{206}Pb/^{204}Pb_{meas}$ = 16·98–17·88; $^{207}Pb/^{204}Pb_{meas}$ = 15·16–15·37) compared with the most unradiogenic (contaminated) East Greenland

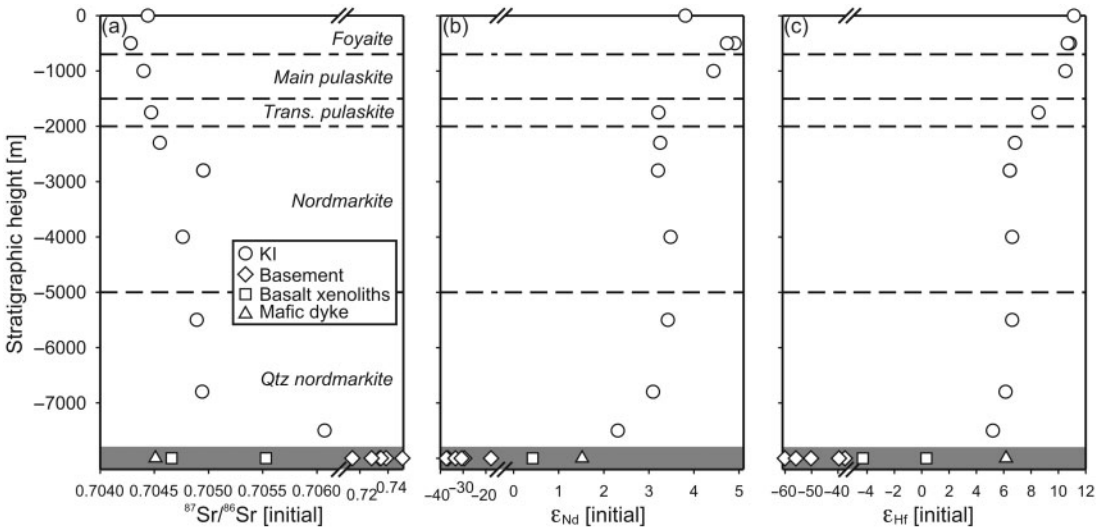

Fig. 7. Whole-rock Sr, Nd and Hf isotope compositions vs stratigraphic height in the Kangerlussuaq Intrusion. Compositions of basement rocks [including data from Riishuus *et al.* (2005)], basaltic xenoliths and dykes are given in the grey band at the base of each plot.

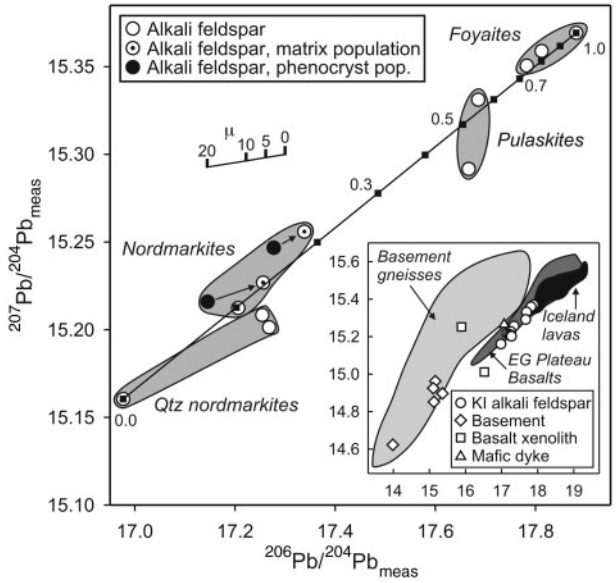

Fig. 8. $^{207}Pb/^{204}Pb_{meas}$–$^{206}Pb/^{204}Pb_{meas}$ isotope compositions of alkali feldspars from the Kangerlussuaq Intrusion, including a simple mixing curve between melt compositions in equilibrium with the earliest, most crustally contaminated quartz nordmarkite (454067) and the foyaites. Mixing end-members: quartz nordmarkite melt ($^{206}Pb/^{204}Pb = 16{\cdot}98$, $^{207}Pb/^{204}Pb = 15{\cdot}16$, Pb = 1 ppm); foyaite melt ($^{206}Pb/^{204}Pb = 17{\cdot}88$, $^{207}Pb/^{204}Pb = 15{\cdot}37$, Pb = 3 ppm). Pb concentrations of mixing end-members are estimated using alkali feldspar trace element concentrations (Table 5) and partition coefficients (Villemant, 1988). Vector shows the effects of age correction to 50 Ma for different μ ($^{238}U/^{204}Pb$) values. Most μ values are in the range 2–16 with an average of eight (a single outlier, sample 454079, has a μ value of 28·5). The analysed alkali feldspar phenocryst and matrix from sample 454097 both have μ values of 11–12, so it appears that the isotopic variation between coexisting alkali feldspar populations is a primary magmatic feature and not related to age-correction. In the inset, compositions of local basement rocks (Riishuus *et al.*, 2005; this study), basaltic xenoliths and mafic dyke are shown for comparison (symbols as in Fig. 8) along with fields of Iceland lavas (Sun & Jahn, 1975; Sun *et al.*, 1975; Cohen & O'Nions, 1982; Park, 1990; Elliott *et al.*, 1991; Furman *et al.*, 1991; Hards *et al.*, 1995; Hanan & Schilling, 1997; Hardarson *et al.*, 1997; Stecher *et al.*, 1999), East Greenland Plateau Basalts (Peate & Stecher, 2003; Peate *et al.*, 2003; Andreasen *et al.*, 2004) and East Greenland regional gneisses (Leeman *et al.*, 1976; Taylor *et al.*, 1992).

Plateau Basalts. The stratigraphic variation from the relatively unradiogenic alkali feldspars in the quartz nordmarkites to more radiogenic alkali feldspars in the foyaites is consistent with the Sr, Nd and Hf isotopic variation towards a weaker crustal signature stratigraphically upwards within the intrusion. Analyses of both phenocryst and matrix alkali feldspar in two nordmarkite samples (454096 and 454097) consistently show that the matrix phase is more radiogenic than the phenocryst phase, beyond the effect of age correction. The dyke and basaltic xenoliths are far less radiogenic than the foyaites ($^{206}Pb/^{204}Pb_{meas} = 15{\cdot}89$–$17{\cdot}01$; $^{207}Pb/^{204}Pb_{meas} = 15{\cdot}01$–$15{\cdot}26$) (Fig. 8 inset).

DISCUSSION

Parental magma

Mafic alkaline magmatism in central East Greenland (Nielsen, 1987) includes: (1) inland alkaline basalts of the Prinsen af Wales Bjerge Formation (55–52 Ma, Peate *et al.*, 2003); (2) the Gardiner complex (56–54 Ma, Waight *et al.*, 2002; Tegner *et al.*, 2008), hosting ultramafic cumulates and a ring-dyke system of evolved alkaline rocks (melilitolites, agpaitic syenites and carbonatites) (Nielsen, 1980, 1981); (3) two suites of mildly alkaline coastal dykes (55–50 Ma and 50–33 Ma, Gleadow & Brooks, 1979) of saturated to undersaturated composition (predominantly alkali basalt and hawaiite) (Nielsen, 1978); (4) the gabbroic Lilloise intrusion of alkali basaltic or picritic parentage (~50 Ma, Brown, 1973; Chambers & Brown, 1995), basanite dykes (37–36 Ma) and nephelinite diatremes (~50 Ma) from the Wiedemann Fjord–Kronborg Gletscher lineament (Nielsen *et al.*, 2001; Tegner *et al.*, 2008); (5) a mildly alkaline ~47 Ma diorite intrusion and trachyandesite pillowed intrusive rocks in the Astrophyllite Bay Complex (2·5% *ne* to 1·1% *qz* normative) (Riishuus *et al.*, 2005).

Kempe & Deer (1976) suggested that the KI parental magma was a mantle-derived alkali olivine basalt, whereas Brooks & Gill (1982) favoured fractionation of a nephelinitic parent to produce the phonolitic melt from which the foyaites crystallized. Unlike the inland Gardiner complex, there is no evidence from the Kangerlussuaq Alkaline Complex for the presence of extremely alkaline and primitive mafic rocks that might indicate differentiation directly from nephelinitic magma to phonolite. Conversely, the presence of alkali olivine basaltic to basanitic dykes and intermediate diorites and trachyandesites within the Kangerlussuaq Alkaline Complex (Riishuus *et al.*, 2005) suggests differentiation from an alkali olivine basalt or basanite parent magma. The composition of aegirine–augite cores in the foyaites ($En_{24–27}Fs_{21–25}Wo_{43–45}Ac_{5–6}$, Table 2) are similar to those in oceanic phonolites from Rarotonga ($En_{23–25}Fs_{23–24}Wo_{42–44}Ac_{9–10}$) inferred to be formed by fractionation of alkali basaltic to basanitic magmas (Thompson *et al.*, 2001). The highly peralkaline rocks of the Ilímaussaq Complex, South Greenland, are taken to represent residues from extreme fractional crystallization in an alkali basaltic parent magma chamber situated deep in the crust (e.g. Larsen & Sørensen, 1987; Stevenson *et al.*, 1997; Markl *et al.*, 2001; Marks & Markl, 2001), giving rise to distinct negative Eu anomalies in the agpaitic rocks (Bailey *et al.*, 1978). Kramm & Kogarko (1994) suggested that the lack of significant Eu anomalies in the rocks of the Khibina and Lovozero alkaline centres of the Kola Peninsula indicate that they formed as residues from nephelinite magmas at mantle pressures. The titanites from the KI display significant negative Eu anomalies in the nordmarkites and either absent or negative Eu anomalies in the pulaskites and foyaites (Fig. 6). The negative

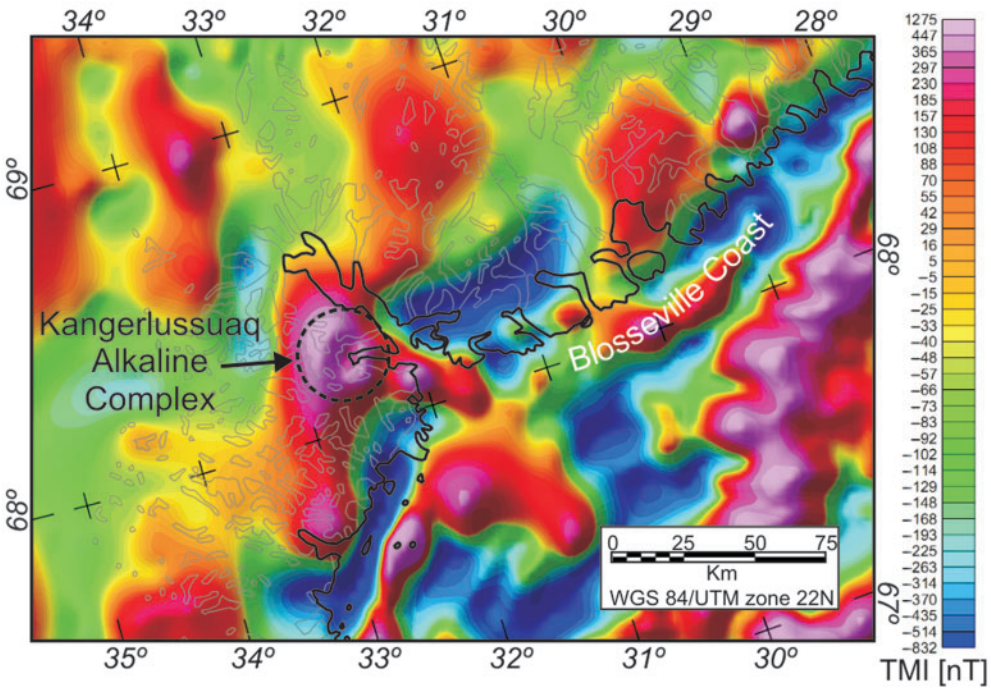

Fig. 9. Total magnetic intensity field of the Kangerlussuaq area after Verhoef *et al.* (1996). The location of the Kangerlussuaq Intrusion coincides with a large positive magnetic anomaly in the left centre. The maximum intensity over the intrusion is ~600 nT and the width of the anomaly is ~60 km.

Eu anomalies of the nordmarkites indicate a 'plagioclase-effect', as do the generally low Sr contents of the KI (11–852 ppm, Table 1 and Fig. 5h) relative to nepheline syenites from the Khibina centre (255–2800 ppm; Kramm & Kogarko, 1994). The low contents of Cr (<5 ppm) and Ni (<7 ppm) in all rock types of the KI suggest olivine and clinopyroxene fractionation (Table 1). Ultimately, a nephelinitic parent appears less likely than a basanitic or alkali basaltic parent magma for the KI.

Structure and volume of plumbing system

The occurrence of kaersutite gabbro inclusions in dykes cross-cutting the KI led Brooks & Platt (1975) to suggest that an alkaline mafic intrusion underlies the Kangerlussuaq Alkaline Complex. This is supported by the total magnetic intensity field in the Kangerlussuaq area (Fig. 9) based on aeromagnetic data from Verhoef *et al.* (1996). The location of the complex coincides with a large positive magnetic anomaly with a maximum intensity of ~600 nT and a width of ~60 km. Normally, the depth of a magnetic anomaly roughly corresponds to half its width. As the East Greenland crust is ~30 km thick (Korenaga *et al.*, 2000; Holbrook *et al.*, 2001; Dahl-Jensen *et al.*, 2003), this magnetic anomaly could represent one or several large mafic bodies situated at various crustal levels below the KI. The magnetic data indicate that the KI is only the surface expression of a much larger magmatic complex at depth in the crust. If fractionation models suggesting that phonolites represent 13–40% residuals of the parent basanite (Kyle, 1981; le Roex *et al.*, 1990; Ablay *et al.*, 1998; Thompson *et al.*, 2001) are considered, then a large volume (10 000–30 000 km^3) of solidified parent magma is required in the crust below to produce the estimated volume (~4000 km^3) of evolved alkaline rocks in the KI (Fig. 10a).

The basaltic xenoliths from the chamber roof

The lavas of the Lower Basalts range from picrite to basaltic andesite with minor occurences of ne-normative lavas, olivine basalt as the most abundant rock type and they vary texturally from aphyric to olivine- and pyroxene-phyric (Nielsen *et al.*, 1981; Fram & Lesher, 1997; Hansen & Nielsen, 1999). The Plateau Basalts are dominantly olivine- and plagioclase-phyric tholeiitic basalts (qtz- or ol-normative) and there are no picrites or basaltic andesites (Larsen & Watt, 1985; Larsen *et al.*, 1989). Comparison with the petrology of the established East Greenland lava sequence suggests that the silica-saturated to -undersaturated, aphyric to pyroxene-phyric basaltic xenoliths found in the KI belong to the Lower Basalts. Field observations of the rounded shapes of the basaltic xenoliths and the presence of reaction zones and small (<10 cm) diffuse mafic bodies in the syenite matrix, but sharp contacts between syenite veins and the interior of the xenoliths indicate minor digestion of the basaltic

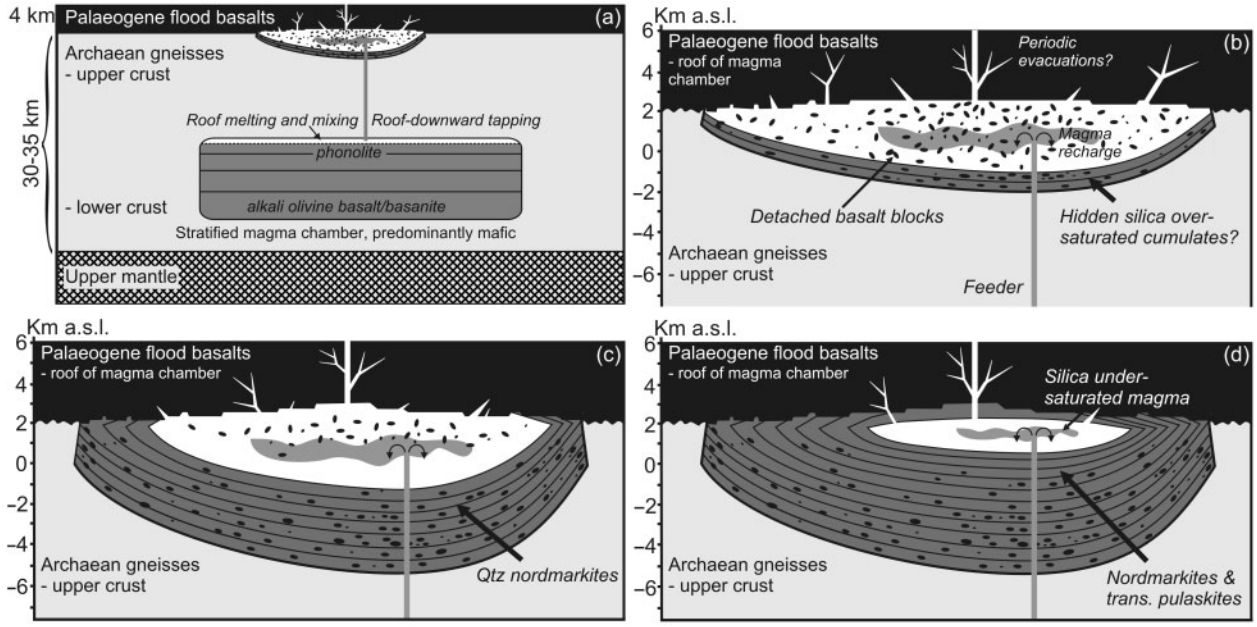

Fig. 10. Schematic illustration of the structural–magmatic emplacement model proposed to explain the petrogenesis of the Kangerlussuaq Intrusion. (a, b) Roof zone melting of gneissic crust above a large zoned magma chamber (stratified from alkali olivine basalt or basanite at floor to phonolite at roof). A silica-oversaturated magma (quartz trachyte) formed as a consequence of contamination and mingling with crustal-derived melt in the roof zone. Roof-downwards tapping of this chamber led to emplacement of an initially silica-oversaturated, lopolithic, sill-like body in the uppermost crust with crystallization of potential hidden cumulates and the outermost exposed quartz nordmarkites. Roof collapse of the unsupported basalts and magma stoping led to incorporation of basaltic xenoliths in the cumulate stratigraphy. Periodic evacuations are likely to have occurred in such a shallow-level, recharged magma chamber. (c) Continued recharge of silica-undersaturated magma is inferred to have driven the resident magma to less silica-oversaturation and led to further stoping of the lava pile, as indicated by the continued presence of basaltic xenoliths through the nordmarkites *sensu lato*. Increased load of the cumulate pile and tapping of the underlying chamber probably led to subsidence of the KI chamber floor, giving a steeper inward slope (30–60°). (d) Continued recharge drove the residual magma to a silica-undersaturated composition, allowing fractionation towards the phonolite minimum. Roof crystallization (and/or decreasing chamber size) stabilized the roof and hindered further incorporation of basaltic xenoliths into the stratigraphy.

xenoliths by the host trachyte magma. Although basaltic xenoliths in gabbros usually show evidence of partial melting, such as LREE depletion and the presence of trapped pegmatitic pods (Brandriss *et al.*, 1996), such evidence is not found in this study; this feature argues against significant anatexis of the basaltic xenoliths by trachyte magma.

Magma chamber model

The field relations, mineralogy and geochemical data presented provide evidence of a series of complex magma chamber processes that require revision of previous models (Wager, 1965; Kempe & Deer, 1976; Pankhurst *et al.*, 1976; Brooks & Gill, 1982) and have wider implications for the formation of coexisting silica-oversaturated and -undersaturated syenites.

Following the field observations by Wager (1965) and later workers of inward-sloping basaltic xenoliths and platy feldspars, and nepheline-bearing pegmatites cutting the nordmarkites and not vice versa, we consider that the KI is a layered intrusion that solidified from the bottom upwards. Although the main heat loss occurred at the top and the sides, cumulus alkali feldspar must have formed or accumulated at the bottom of the chamber, which implies convective circulation of the magma. Had convection not taken place the magma would have solidified from the top downwards; however, the prominent trains of basaltic xenoliths originating from collapses of the roof, and present from the quartz nordmarkites through to the pulaskites, rule this out. One could envisage that between the repeated roof collapses, periods of recurrent top-downwards crystallization might have taken place, but unfortunately the roof zone is not preserved. Layered syenitic intrusions are not uncommon. Magmatic convection coupled with crystal settling has been proposed for the Lovozero alkaline complex (e.g. Kogarko & Khapaev, 1987; Kogarko *et al.*, 2002, 2006), and there is evidence that cumulates formed on both the roof and floor of the Ilímaussaq alkaline intrusion (e.g. Larsen & Sørensen, 1987; Sørensen & Larsen, 1987; Bailey *et al.*, 2006) and the Klokken intrusion (e.g. Parsons, 1979; Parsons & Becker, 1987).

The radiogenic isotopic compositions of the KI clearly testify to an increasing crustal component from the foyaites

through the quartz nordmarkites (Figs 7 and 8) and require involvement of a crustal contamination process in the petrogenesis of the magmas. In a study of the temporal evolution of the Kangerlussuaq Alkaline Complex, Riishuus *et al.* (2006) suggested that the evolved alkaline rocks formed as products of AFC (DePaolo, 1981) between a magmatic end-member intermediate to the Plateau Basalts (Peate & Stecher, 2003; Andreasen *et al.*, 2004) and the alkalic Prinsen af Wales Bjerge Formation basalts (Peate *et al.*, 2003) ($^{87}Sr/^{86}Sr_i = 0{\cdot}7035$, $Sr = 300$ ppm; $\varepsilon_{Ndi} = 6{\cdot}5$, $Nd = 30$ ppm; $\varepsilon_{Hfi} = 13{\cdot}5$, $Hf = 5$ ppm) and varying proportions of two different local contaminants, granulite-facies gneiss ($^{87}Sr/^{86}Sr_{50\ Ma} = 0{\cdot}706$, $Sr = 500$ ppm; $\varepsilon_{Nd,\ 50\ Ma} = -38$, $Nd = 20$ ppm; $\varepsilon_{Hf,\ 50\ Ma} = -65$, $Hf = 2{\cdot}5$ ppm) and amphibolite-facies gneiss ($^{87}Sr/^{86}Sr_{50\ Ma} = 0{\cdot}750$, $Sr = 260$ ppm; $\varepsilon_{Nd,\ 50\ Ma} = -36$, $Nd = 5$ ppm; $\varepsilon_{Hf,\ 50\ Ma} = -65$, $Hf = 2{\cdot}5$ ppm) (Taylor *et al.*, 1992; Riishuus *et al.*, 2005; this study). Using these end-members and an r value (rate of assimilation/rate of crystallization) of 0·3, the observed large variations in the Sr–Nd–Hf isotope compositions in the KI can be produced when 15–45% of the initial liquid has solidified (Riishuus *et al.*, 2006). The consistent relationship of more radiogenic Pb isotope compositions in matrix alkali feldspars compared with coexisting alkali feldspar phenocrysts (Fig. 8) suggests involvement of magma recharge. We propose a model for the petrological and geochemical evolution of the magma chamber that includes fractional crystallization, magma recharge and crustal assimilation. The model is discussed below and illustrated in Fig. 10.

The outer part of the KI, hosting the quartz nordmarkites, represents the earliest known cumulates formed after emplacement of magma into the chamber at the contact between the Archaean basement gneisses and the overlying Palaeogene flood basalts. The lower quartz nordmarkites (e.g. 454067, −7500 m) clearly host two populations of pyroxene and amphibole as inclusions in alkali feldspar phenocrysts and in interstitial pockets, and two alkali feldspar populations as large zoned phenocrysts and in the groundmass (Fig. 3a and b). The close resemblance between alkali feldspar-hosted aegirine–augite and amphibole inclusions in the quartz nordmarkites (454067) and aegirine–augites in the foyaites and amphiboles in the pulaskites could suggest crystallization from similar melt compositions (Figs 4b and c, Tables 1 and 2). This is in strong contrast with the more evolved groundmass pyroxene (Fig. 4b), amphibole (Fig. 4c) and alkali feldspar matrix compositions (Table 5), higher whole-rock SiO_2 (Fig. 5a), REE and Ta in titanite (Fig. 6 and Table 4), Fe in alkali feldspar (Table 5), and lower V contents (Fig. 5e) of the same quartz nordmarkite sample when compared with the pulaskites and foyaites. Furthermore, the Sr–Nd–Hf–Pb isotope data clearly show that the quartz nordmarkite

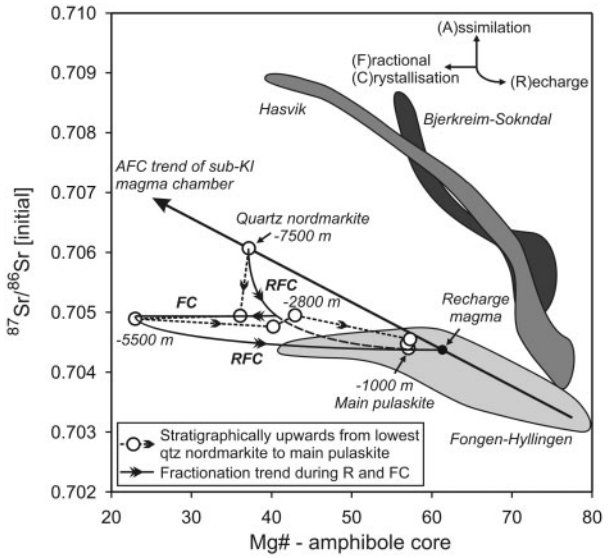

Fig. 11. Variation of whole-rock $^{87}Sr/^{86}Sr_i$ with Mg-number in amphibole cores for the quartz nordmarkites through to the main pulaskites from the Kangerlussuaq Intrusion. A possible coupled assimilation and fractional crystallization (AFC) trend for the inferred stratified magma chamber below the Kangerlussuaq Intrusion is indicated by the bold black arrow. The $^{87}Sr/^{86}Sr_i$ and Mg-number of the stratigraphically lowest quartz nordmarkite is produced by tapping of the most evolved and contaminated part of the underlying chamber. The stratigraphic variations above this level can qualitatively be produced by periodic magmatic recharge and fractional crystallization (RFC) and FC alone, giving the most evolved Mg-number, followed by periodic RFC to produce the increasingly primitive and less contaminated nordmarkites and pulaskites. For simplicity, the recharge magma composition remains fixed in this model. The Sr content of the recharge magma is far greater than that of the residual magma, hence the curvature of the RFC trends. As an alternative model, the recharge magma continuously changed composition (not shown) following a trend opposite to the AFC trend predicted for the sub-KI magma chamber. Data from layered intrusions where AFC has been suggested are shown for comparison; Hasvik (Mg-number$_{opx}$, Tegner *et al.*, 1999), Bjerkreim–Sokndal (Mg-number$_{opx}$, Nielsen *et al.*, 1996) and Fongen–Hyllingen (Mg-number$_{cpx}$, Sørensen & Wilson, 1995). The upwards stratigraphic sequence through the layered series in these intrusions is from right to left in the diagram.

(454067) has a much larger crustal component than the foyaites (Figs 7 and 8) and indicate that crustal contamination played an important role. Contaminated layered gabbroic intrusions with AFC trends (Fig. 11) often contain abundant xenoliths of metabasalts, metasediments and gneisses (Sørensen & Wilson, 1995; Nielsen *et al.*, 1996; Tegner *et al.*, 1999), whereas syenites with xenoliths of local wall-rock show evidence of *in situ* assimilation during final emplacement that led to significant but only local effects (Marks & Markl, 2001). The thermal budget between trachyte magma and its country rock is less favourable for assimilation to take place than when basaltic magma is considered. Hence, the lack of gneissic xenoliths in the quartz nordmarkites indicates that little or no *in situ* assimilation of gneiss took place at the final emplacement level.

As gneiss is the only available crustal contaminant that is able to produce the radiogenic isotope composition of the quartz nordmarkites, we argue that most contamination must have taken place at a deeper crustal level. The AFC modelling by Riishuus *et al.* (2006) showed that the KI is dominated by contamination with lower crustal granulite-facies gneisses. We suggest that silica-oversaturated magma formed as a consequence of contamination of an initially silica-undersaturated melt, not unlike the melt from which the foyaites crystallized, by silica-rich gneisses in the roof zone of a large, stratified, deep-seated magma chamber below the present KI (Fig. 10a). By tapping from the roof zone and downwards into this chamber, the KI developed as an initially silica-oversaturated, lopolithic, sill-like body emplaced in the uppermost crust (Fig. 10a and b). The outermost quartz nordmarkites crystallized as the earliest cumulates in this lopolith, after any hidden cumulates (Fig. 10b and c).

The up-section increase in whole-rock SiO_2 content (Fig. 5a) and decrease in Al_2O_3 content (Fig. 5b), whole-rock Mg-number (Fig. 5d) and amphibole Mg-number (Fig. 4c) from −7500 m to −5500 m suggest initial fractionation of the residual magma towards the silica-oversaturated minimum. Despite crystallization of accessory titanite and zircon, acting as REE and HFSE sinks, the concentrations of incompatible trace elements increase upwards into the nordmarkites (Figs 5f, g and 6) and could indicate that the magma became more evolved. In contrast, decreasing $^{87}Sr/^{86}Sr_i$ (Fig. 7a) and increasing ε_{Ndi}, ε_{Hfi}, $^{206}Pb/^{204}Pb_{meas}$ and $^{207}Pb/^{204}Pb_{meas}$ (Figs 7b, c and 8) show that, during the same interval, the magma also became less contaminated. This implies mixing between the resident magma and a less contaminated melt, which we suggest was derived from a lower level of the underlying chamber (Fig. 10a). The variation of Mg-number in amphibole cores with whole-rock Sr isotope composition up through the stratigraphy is opposite to the trend developed in layered intrusions that have undergone AFC (Fig. 11). If the stratigraphically lowest quartz nordmarkite crystallized directly from an evolved melt tapped from an underlying, stratified magma chamber it should plot on the AFC trend of this sub-KI chamber. Periodic recharge (with less evolved and less contaminated melt from the sub-KI chamber) and fractional crystallization (RFC) followed by FC alone could explain the stratigraphic variations towards the lowest Mg-number of amphibole cores. Injection of fresh magma would result in expansion and/or tapping of the KI magma chamber. The numerous basaltic xenoliths (Fig. 2a) in the nordmarkites *sensu lato* suggest expansion of the chamber by stoping into the lava sequence forming the chamber roof (Wager, 1965). We have no evidence for eruptions of trachytic to phonolitic material, but intuitively it is hard to envisage that such a large, shallow chamber was not periodically tapped.

The stratigraphic sequence from the base of the nordmarkites through the main pulaskites (−1000 m) is characterized by upwards decreasing whole-rock SiO_2, Zr and Ce (Fig. 5a, f and g), titanite REE and Ta (Fig. 6 and Table 4) and alkali feldspar Fe (Table 5) contents, and increasing whole-rock Al_2O_3, V contents (Fig. 5b and e), whole-rock Mg-number (Fig. 5d) and amphibole Mg-number (Fig. 4c). We believe that this indicates crystallization from an increasingly primitive and silica-poor magma. Upsection decreasing $^{87}Sr/^{86}Sr_i$ and increasing ε_{Ndi}, ε_{Hfi} (Fig. 7) and Pb isotope compositions (Fig. 8) imply periodic recharge by less contaminated, silica-undersaturated melt (Fig. 11). The Pb isotope compositions of coexisting phenocryst and matrix alkali feldspars show that the matrix phase is more radiogenic than the phenocryst phase (Fig. 8), beyond the effect of age-correction, thereby supporting a periodic recharge–mixing model. The common porphyritic texture of the nordmarkites *sensu lato* may, in fact, be a consequence of multiple magma influxes and intervening stages of cooling, during which crystallization of feldspar was repeatedly halted and renewed, leading to at least two feldspar populations within the nordmarkites. From the level where the basaltic xenoliths cease to be present (lower part of the main pulaskites) we believe that the magma chamber, now dramatically reduced in size, was effectively shielded from its country rock envelope as a result of crystallization downwards from the roof (Fig. 10d).

The transition from the main pulaskites into the foyaites in the uppermost part of the succession shows a marked decrease in SiO_2 (~63–64 to 55–58 wt %) and marked increases in Al_2O_3 (~18 to 21–23 wt %), total alkalis (~13 to 16 wt %) and pyroxene Mg-number (1–2 to 18–59). As no intrusive contacts have been found, the marked chemical changes could be explained by a major magma recharge relative to the resident melt. As the lowest $^{87}Sr/^{86}Sr_i$ values and highest ε_{Ndi}, ε_{Hfi}, $^{206}Pb/^{204}Pb_{meas}$ and $^{207}Pb/^{204}Pb_{meas}$ values are found in the foyaites, the last part of the KI to crystallize formed from the most primitive, least crustally contaminated melt. The final recharge magma tapped from the underlying chamber must have been essentially uncontaminated mafic phonolite.

Magma mixing model

To evaluate how the sample suite conforms to the proposed magma mixing model, we have constructed simple mixing curves for the variation in Sr, Hf and Pb isotopes between a crustally contaminated quartz trachytic melt in equilibrium with the first formed quartz nordmarkites and a silica-undersaturated melt in equilibrium with the foyaites (Figs 8 and 12). The exact composition of the recharge magma is unknown, as the foyaites are likely to have crystallized from mixed magmas themselves. Nevertheless, based on their isotopic composition, the foyaites represent

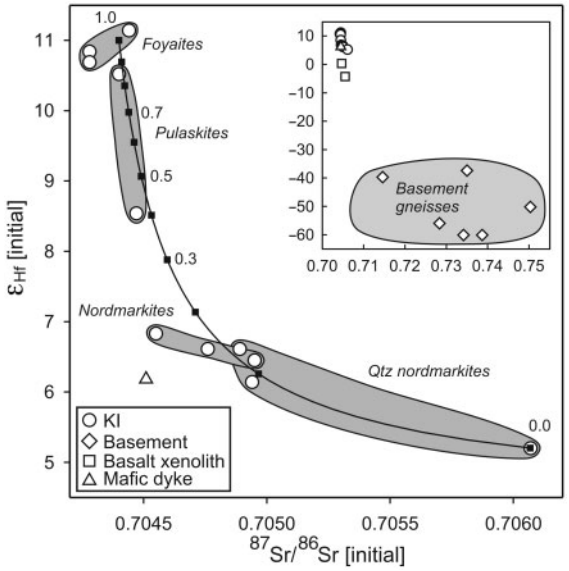

Fig. 12. $^{87}Sr/^{86}Sr_i$–ε_{Hfi} isotopic variations in the Kangerlussuaq Intrusion, including a simple mixing curve between melt compositions in equilibrium with the earliest, most crustally contaminated quartz nordmarkite (454067) and the foyaites. Mixing end-members: quartz nordmarkite melt ($^{87}Sr/^{86}Sr_i = 0{\cdot}7061$, Sr = 8·5 ppm, $\varepsilon_{Hfi} = +5{\cdot}2$, Hf = 3·1 ppm) and foyaite melt ($^{87}Sr/^{86}Sr_i = 0{\cdot}7044$, Sr = 185 ppm, $\varepsilon_{Hfi} = +11$, Hf = 9·8 ppm). Sr and Hf concentrations in end-member melts are estimated using alkali feldspar and titanite trace element concentrations, respectively, and appropriate partition coefficients (Villemant, 1988; Lynton *et al.*, 1993). The strong curvature of the mixing curve results from the contrasting Sr concentrations. Compositions of basement rocks [including data from Riishuus *et al.* (2005)], basaltic xenoliths and a mafic dyke are also indicated.

the most primitive and uncontaminated syenites of the intrusion. The Sr, Hf and Pb concentrations of the KI magma at different stratigraphic levels can be estimated using titanite and alkali feldspar trace element concentrations (Tables 4 and 5) and appropriate mineral/melt partition coefficients (Villemant, 1988; Lynton *et al.*, 1993). The end-member melt compositions are based on the most contaminated and stratigraphically lowest quartz nordmarkite (454067) ($^{87}Sr/^{86}Sr_i = 0{\cdot}7061$, Sr = 8·5 ppm; $\varepsilon_{Hfi} = +5{\cdot}2$, Hf = 3·1 ppm; $^{206}Pb/^{204}Pb = 16{\cdot}98$, $^{207}Pb/^{204}Pb = 15{\cdot}16$, Pb = 1 ppm), and the least contaminated and stratigraphically highest foyaite (454089) with a slight sway from the other foyaite samples ($^{87}Sr/^{86}Sr_i = 0{\cdot}7044$, Sr = 185 ppm, $\varepsilon_{Hfi} = +11$, Hf = 9·8 ppm; $^{206}Pb/^{204}Pb = 17{\cdot}88$, $^{207}Pb/^{204}Pb = 15{\cdot}37$, Pb = 3 ppm). The KI samples fall very close to the calculated mixing lines for both Pb (Fig. 8) and Sr–Hf (Fig. 12), supporting the view that the silica-oversaturated and -undersaturated KI rocks are related through periodic magma recharge. The isotopic composition of single samples is produced by similar mixing ratios in Sr–Hf and Pb isotope space, which adds further support for the mixing model and validity of the end-member parameters.

Phase equilibrium evolution—the thermal barrier

Any petrogenetic model attempting to explain the evolutionary trend of the KI should be consistent with phase equilibrium constraints. The possibilities for changing the magma from a silica-oversaturated to a silica-undersaturated composition by isothermal magma mixing can be evaluated using isothermal sections in Petrogeny's Residua System at 1 kbar $P(H_2O)$ (Fig. 13). Alkali feldspar compositions *F1* (Or_{38}), *F2* (Or_{36}), *F3′* (Or_{41}) and *F4′* (Or_{55}) in Fig. 13a and b correspond to groundmass alkali feldspar compositions based on $\bar{2}01$ spacing X-ray analyses of nordmarkites, transitional pulaskites, main pulaskites and foyaites, respectively, from Kempe & Deer (1970). Let us consider a hypothetical initial bulk composition *X* ($Q_6Ab_{60}Or_{34}$) consisting of alkali feldspar composition Or_{38} (*F1*) and liquid *L1* (Fig. 13b), and two hypothetical silica-undersaturated recharge magma compositions, *C* and *C′*, that can give rise to the observed alkali feldspar compositions when mixed with the initial bulk *X*. At 850°C (Fig. 13a–c), the *L1* temperature is below the alkali feldspar saddle minimum [865°C, 1 kbar $P(H_2O)$] with solid solution crossing the Ab–Or syenite divide. By recharge with *C*, the alkali feldspar composition will change from *F1* to *F2*, and the initial liquid *L1* will change composition and eventually disappear, leaving *F2* as the only phase present. If more *C* could be mixed with the completely solid *F2*, a silica-undersaturated melt *L2* would be produced at first, followed by a superheated liquid. By recharge with *C′*, *L1* will be consumed, leaving alkali feldspar (with a slightly more Or-rich composition than *F1*) as the only phase present. Again, if more *C′* could be mixed with the alkali feldspar phase, a silica-undersaturated melt *L3′* would be developed and coexist with alkali feldspar *F3* at bulk composition *B3′*. Increasingly Or-rich alkali feldspar will develop with further addition of *C′*, and when the bulk composition is identical to *L4′*, alkali feldspar *F4′* disappears.

If the temperature is raised only 20°C to 870°C (Fig. 13d), slightly above the alkali feldspar minimum (865°C), the silica-oversaturated and -undersaturated liquid fields are joined. Recharge of the initial bulk composition with *C* or *C′* at this temperature would let the bulk composition cross the Ab–Or join, without intersecting the solidus. Once the bulk composition crosses the Ab–Or join it will eventually terminate at the nepheline syenite minimum (Fig. 13e). At these conditions the recharge magma would be superheated and probably at a higher temperature than the resident magma to raise the bulk temperature above the thermal barrier. The continuous normative compositional transition across the Ab–Or join from nordmarkite to pulaskite suggests that the bulk magma was either kept at the liquidus or elevated above the liquidus

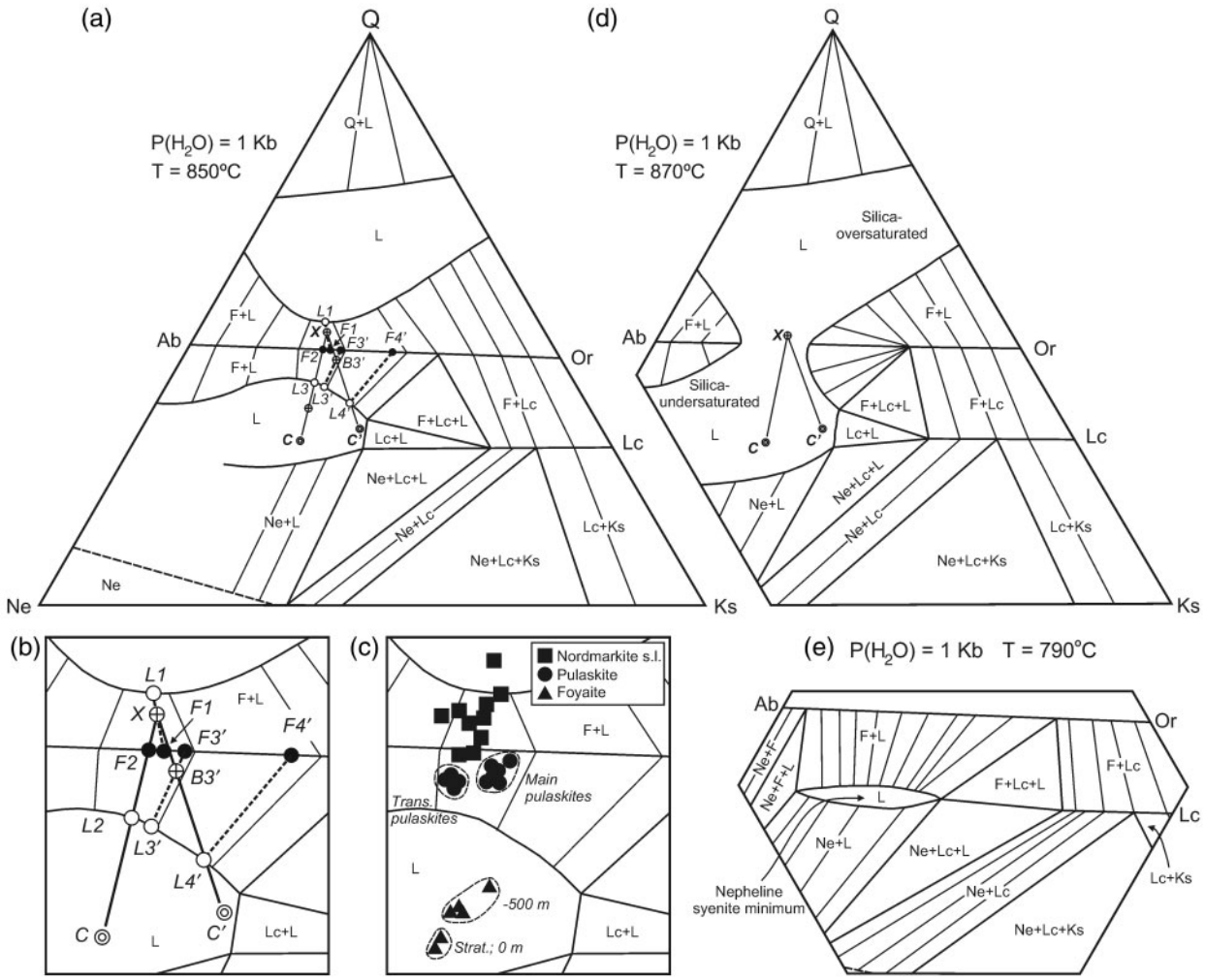

Fig. 13. Isothermal sections of Petrogeny's Residua System for 850°C (a, b, c), 870°C (d) and 790°C (e) after Fudali (1963). (a, b) The changing phase compositions for an initial silica-oversaturated magma (*X*) being mixed with a silica-undersaturated melt of either composition *C* or *C*′. *L*, *F* and *B* are liquid, alkali feldspar and contaminated bulk compositions, respectively, related to *C*. *L*′, *F*′ and *B*′ relate to *C*′. Numerals represent compositions at same time interval (e.g. *L3*′, *F3*′ and *B3*′). Dashed lines are tie lines between feldspar compositions and their equilibrium liquids. (c) The normative compositions of syenites from the KI (this study; all samples with >87% of the ternary components) projected into Petrogeny's Residua System. Two nordmarkites plotting below the Ab–Or join contain silica-undersaturated mafic silicates. (d) Mixing lines between superheated liquids *X* and *C* or *C*′.

in small increments before returning to it and precipitating alkali feldspar again. Overcoming the thermal barrier may be aided by depression of the liquidus surface by elevation of the vapour pressure (e.g. Tuttle & Bowen, 1958; Morse, 1969), as discussed in relation to the KI by Kempe & Deer (1976) and Pankhurst *et al.* (1976). This is supported by an oxygen and hydrogen isotope study of the KI indicating release of water with a meteoric origin into the syenite magma by dehydration of hydrothermally altered basaltic xenoliths (Riishuus *et al.*, in preparation).

The decreasing amphibole (Fig. 4c) and whole-rock (Fig. 5d) Mg-numbers and increasing whole-rock SiO_2 content (Fig. 5a) up through the quartz nordmarkites indicate that the KI magma initially fractionated towards the granite minimum, despite being mixed with less crustally contaminated material as suggested by the Sr–Nd–Hf–Pb isotopic variation (Figs 7 and 8). This implies an initial relatively low recharge/resident magma ratio, followed by an increasing ratio after formation of the quartz nordmarkites, forcing the bulk magma back towards the Ab–Or join.

The exact liquid evolution of the KI is difficult to establish, as the compositions and temperatures of the initial residual and recharge magmas are unknown. Recharge with *C* will satisfy the alkali feldspar compositional change from the nordmarkites (*F1* = Or_{38}) to the transitional pulaskites (*F2* = Or_{36}), but will not be able to produce a liquid composition in equilibrium with *F3* (Or_{41}) of the main pulaskites (Fig. 13b). On the other hand, recharge with *C*′ cannot produce the *F2* in equilibrium

with the transitional pulaskites, but can produce a bulk composition close to the normative composition of the main pulaskites and a liquid in equilibrium with *F3′* (Fig. 13b and c). This relationship suggests that the recharge magma changed composition between formation of the transitional and main pulaskites. The large compositional jump between the main pulaskites and the foyaites must result from a further increase in the recharge/residual magma ratio (Fig. 13c). The location of the normative compositions of the foyaites in extension of the *F4′–L4′* tie line shows that the foyaites from −500 m and 0 m can be related through fractionation of the remaining melt that crystallized alkali feldspar with Or_{55} (Fig. 13b and c).

Comparison with other alkaline complexes

Several major syenite complexes resemble the KI in showing temporal evolution from early (outer) quartz syenites or monzonites to later (inner) nepheline syenites.

The 178 Ma Marangudzi ring complex (~80 km^2), SE Zimbabwe, formed during the waning stage of Karoo flood basalt volcanism and consists, in order of intrusion, of a gabbro body, quartz syenite ring dykes and nepheline monzonite or syenite cone sheets (e.g. Foland & Henderson, 1976; Foland *et al.*, 1993). The quartz syenites have high $^{87}Sr/^{86}Sr$ and low $^{143}Nd/^{144}Nd$ values, whereas the nepheline syenites have low $^{87}Sr/^{86}Sr$ and high $^{143}Nd/^{144}Nd$ values (Foland *et al.*, 1993). The entire suite seems to converge at a common low $^{87}Sr/^{86}Sr$ and high $^{143}Nd/^{144}Nd$ composition; this feature led Foland *et al.* (1993) to suggest an origin from a common silica-undersaturated parental magma. Their model involves development of the quartz syenites from felsic, silica-undersaturated melts undergoing assimilation of felsic crust and fractional crystallization, whereas the nepheline syenites formed by closed-system fractional crystallization alone or with only minor contamination.

The alkaline core of the 131–127 Ma Messum complex in NW Namibia, part of the Paraná–Etendeka flood basalt province, consists of an outer quartz syenite suite and an inner silica-undersaturated suite dominated by nepheline syenite (e.g. Harris *et al.*, 1999). The core is surrounded by older gabbros. The Messum felsic alkaline core is only 6 km in diameter and therefore much smaller than the KI. The quartz syenites (cut by undersaturated dykes) are presumably older than the undersaturated syenites but the contact between them is not exposed. Conversely, the centre of the complex suggests a gradation from nepheline syenite through nepheline-poor syenite to syenite and quartz syenite. Ultimately, it remains unclear whether the alkaline core formed from one or several bodies. Sr and O isotope data indicate a decreasing effect of crustal contamination with time, favouring progressive armouring of the magmatic plumbing system by less contaminated material (Harris *et al.*, 1999).

The very large larvikite–lardalite complex (monzonite–nepheline syenite) (~1000 km^2) of the Permian rift-system in the Oslo district, Norway, displays at least eight ring structures, identified on the basis of topographic features, orientation fabrics (igneous lamination or modal layering), contact relations and aeromagnetic properties. They cut each other in a pattern suggesting a general shift of magmatic focus from east to west (Petersen, 1978). Compositional variations in the larvikite complex from silica-oversaturated, through larvikites with neither quartz nor nepheline, to silica-undersaturated larvikites follow the pattern of structural younging towards the west. The lardalites constitute the core of the complex and display conspicuous contact zones with dendritic growth of alkali feldspar, nepheline and pyroxene along internal contacts and against the earlier larvikites, supporting an origin of the entire complex by multiple injections (Petersen, 1978, 1985).

The 1130 Ma Ilímaussaq Complex (17 km × 8 km) consists of an early silica-undersaturated augite syenite intruded by an alkali granite sheet and followed by a later series dominated by layered, agpaitic nepheline syenites (Ferguson, 1964). The magmas leading to the intrusive events of Ilímaussaq have been related to fractional crystallization and crustal assimilation of a stratified alkali basaltic magma deeper in the crust, before ascending to their present level, where further assimilation and extreme fractionation took place (e.g. Larsen & Sørensen, 1987; Markl *et al.*, 2001; Marks & Markl, 2001). Based on whole-rock Nd isotope data Stevenson *et al.* (1997) suggested that, during the evolution of the complex, the degree of crustal assimilation changed from 12% in the augite syenite, over 35–40% in the alkali granite, to 17% in the agpaitic rocks with respect to the initial mass of magma. Mineral Nd and O isotope compositions led Marks *et al.* (2004) to favour a model in which both the augite syenite and the agpaitic rocks of the Ilimaussaq complex evolved in a closed system without significant contamination, whereas the alkali granite developed from parts of the augite syenite magma that became contaminated with lower crust (13% bulk assimilation) during ascent.

The Marangudzi and Ilímaussaq complexes are clearly made up of discrete intrusive bodies. The Oslo Rift larvikite–lardalite complex also formed as a series of separate intrusions, whereas contact relations between the syenites of the Messum complex are unclear. Wager (1965) did not find any internal intrusive contacts in the KI and reported a gradual transition from the quartz nordmarkites to the foyaites. In comparison with the models proposed for the Marangudzi ring complex and the Messum alkaline core, where the suites of coexisting quartz and nepheline syenites formed as distinct intrusions from initially silica-undersaturated melts that underwent decreasing amounts of contamination, our favoured model for the KI involves

replenishment of an initially silica-oversaturated, crustally contaminated and continuously fractionating magma by multiple injections of salic, silica-undersaturated melt from the roof zone of an underlying, evolving, stratified magma chamber in the lower crust. We suggest that the earliest known silica-oversaturated KI magma, from which the quartz nordmarkites crystallized, formed by a process similar to that suggested by Foland *et al.* (1993) and Harris *et al.* (1999). Our petrogenetic emplacement model has similarities to the favoured model for the Ilímaussaq Complex (e.g. Larsen & Sørensen, 1987), but the much larger KI formed from a single, long-lasting intrusive event with (1) repeated magmatic recharge leading to progressively less contaminated syenites, (2) nepheline syenites being subordinate in volume to quartz syenites, and (3) absence of differentiation to the extreme agpaitic compositions of Ilímaussaq. Like the KI (Fig. 9), the Messum (Bauer *et al.*, 2003), Larvik (Ramberg & Smithson, 1971) and Ilímaussaq (Blundell, 1978; Forsberg & Rasmussen, 1978) complexes are associated with geophysical anomalies suggesting large, dense structures at depth. It therefore seems to be a general feature that many syenitic intrusions represent the upper crustal expressions of larger, dominantly mafic, underlying igneous complexes.

The temporal evolution in silica content and ε_{Ndi} of a series of alkaline complexes with cogenetic silica-oversaturated and -undersaturated syenites, including the whole Kangerlussuaq Alkaline Complex (e.g. Riishuus *et al.*, 2006), is summarized in Fig. 14. The complexes all demonstrate a clear negative correlation of ε_{Ndi} with the degree of silica saturation, and it is evident that they developed from early, crustally contaminated quartz syenites to late, less contaminated nepheline syenites. This is generally interpreted as assimilation of fusible crustal material during establishment of the plumbing system. It appears to be a general rule that following tapping of contaminated, trachytic to rhyolitic melts to higher crustal levels or eruption, an increasingly shielded plumbing system will then be able to develop uncontaminated, phonolitic melts. Alkaline complexes such as those included in Fig. 14 are typically characterized by marginal quartz syenites and central nepheline syenites, and the KI is a classic example of such a structure (Fig. 1b). The Kangerlussuaq Alkaline Complex as a whole, however, differs from this pattern, as the youngest satellite intrusions are silica-oversaturated (Fig. 14). These intrusions are located SE of the Kangerlussuaq Intrusion (Fig. 1b) and therefore indicate that relocation of the plumbing system took place with the possibility for renewed contamination (Fig. 14), and that prolonged magmatic activity at a fixed location appears to be a requirement for phonolitic magma to reach the upper continental crust (Riishuus *et al.*, 2006).

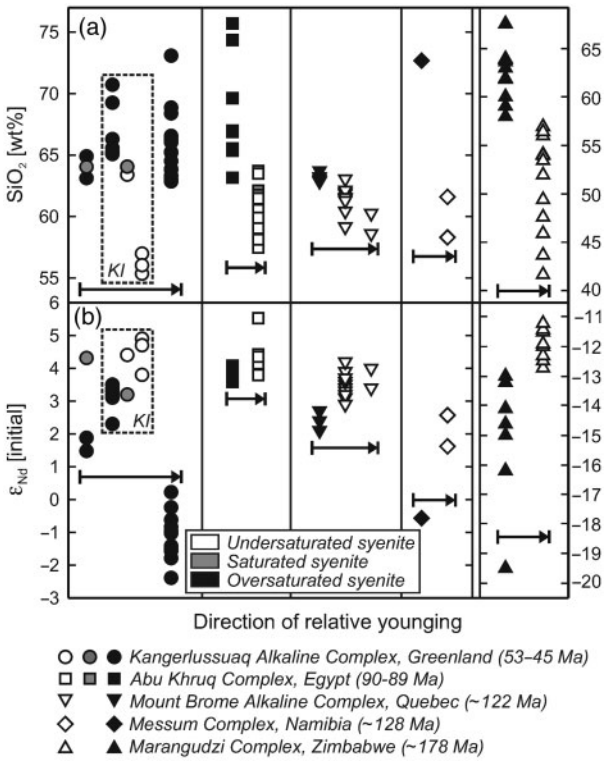

Fig. 14. The relative, temporal evolution of (a) SiO_2 contents and (b) ε_{Ndi} compositions for a compilation of alkaline complexes hosting both silica-oversaturated and -undersaturated syenites. Data from the following complexes are included: Kangerlussuaq Alkaline Complex (Riishuus *et al.*, 2005, 2006; this study), Abu Khruq Complex (Landoll *et al.*, 1994), Mount Brome Alkaline Complex (Chen *et al.*, 1994), the Messum Complex (Harris *et al.*, 1999) and the Marangudzi Complex (Foland *et al.*, 1993).

To the authors' knowledge no examples of layered intrusions with a complete compositional span from gabbro to nepheline syenite have been documented. However, indirect evidence for such compositional variation is found in the Proterozoic Gardar Province in southern Greenland, where composite giant dykes with mafic margins and no internal chilled contacts to granitic, quartz syenitic or nepheline syenitic centres testify to the presence of contemporaneous magmas of contrasting compositions prior to emplacement in the upper crust, implying the presence of an underlying, compositionally zoned magma chamber (e.g. Upton *et al.*, 1985, 2003; Upton, 1987; Halama *et al.*, 2004). Furthermore, successions of increasingly primitive intrusions for both undersaturated (South Qôroq and Motzfeldt) and oversaturated (Kûngnât) complexes (Stephenson & Upton, 1982) are interpreted as representing the periodic tapping of deeper levels of compositionally stratified magma chambers. The tephra succession of the Quaternary Laacher See volcano in Germany, part of the alkaline province of Central Europe, extends from differentiated phonolite to later mafic phonolites, implying an

eruptive mechanism whereby magma was tapped from successively deeper parts of a compositionally zoned, phonolitic magma chamber (e.g. Bogaard & Schmincke, 1984; Wörner & Schmincke, 1984; Harms & Schmincke, 2000; Harms *et al.*, 2004). The last eruptive products were heterogeneous hybrids of phonolite and basanite, the latter having been injected into the base of the magma chamber (Wörner & Wright, 1984). These occurrences of both plutonic and volcanic rocks formed by the tapping of progressively deeper parts of compositionally stratified, alkaline magma chambers add further validation for similar processes to have operated in the petrogenesis of the Kangerlussuaq Intrusion.

CONCLUSIONS

(1) The Kangerlussuaq Intrusion is a large, felsic, alkaline layered intrusion that becomes progressively less contaminated and more primitive from the lower quartz nordmarkites to the upper foyaites. Aeromagnetic data indicate that the Kangerlussuaq Intrusion is only the surface expression of a very large, underlying alkaline mafic–felsic complex. We favour a model in which assimilation of Archaean crust in the roof zone of a large, stratified, alkaline olivine basaltic to basanitic magma chamber, emplaced in the crust below the Kangerlussuaq Intrusion, led to the development of a silica-oversaturated nordmarkitic liquid. The heat required to assimilate the gneisses was provided by the latent heat of crystallization of underlying mafic cumulates. The first melts to be emplaced in the Kangerlussuaq Intrusion magma chamber, from which the quartz nordmarkites and any hidden silica-oversaturated cumulates formed, were tapped from the uppermost roof zone of the underlying chamber. The undersaturated, primitive, basic magma of this chamber, unable to assimilate gneiss because of armouring, fractionated towards a phonolitic composition.

(2) The driving force producing the transition from silica-oversaturated to -undersaturated syenites in the Kangerlussuaq Intrusion chamber was the periodic recharge of uncontaminated, or only slightly contaminated, phonolitic melt that was tapped from the underlying stratified chamber. Mixing of the resident magma in the Kangerlussuaq Intrusion with phonolitic recharge melts resulted in transitional liquid compositions and gradually forced the bulk composition to become undersaturated. The recharge magma had to be hot enough to superheat the bulk magma to overcome the thermal barrier in Petrogeny's Residua System. Alternatively, or operating simultaneously, increasing water pressure, produced by dehydration of basaltic xenoliths as the magma stoped into the roof, superheated the magma to allow the resident and recharge liquids to mix and solidify forming a range of compositions. The last liquids to reach the Kangerlussuaq Intrusion chamber were pristine phonolites produced directly by differentiation of the parent alkali basalt or basanite that gave rise to the foyaites.

(3) Decreasing amphibole and whole-rock Mg-numbers, and increasing SiO_2 content, up through the quartz nordmarkites indicate that the Kangerlussuaq Intrusion magma initially fractionated towards the granite minimum in Petrogeny's Residua System. Increasing recharge/resident magma ratio after formation of the quartz nordmarkites forced the bulk magma back towards the Ab–Or join. The large compositional jump between the main pulaskites and the foyaites may result from a further increase in the recharge/resident magma ratio.

(4) Unlike other occurrences of silica-oversaturated and -undersaturated syenites, in which the different lithologies formed as discrete intrusions, the Kangerlussuaq Intrusion appears to have formed in an open-system, periodically recharged and fractionating magma chamber.

ACKNOWLEDGEMENTS

We thank Tod E. Waight, Joel A. Baker and David G. Ulfbeck for help and technical support with the radiogenic isotope analyses, and Thorkild Rasmussen and Bo Møller Nielsen for access to geophysical data. Sidsel Grundvig, Ingrid Aaes and Jette Villesen are thanked for their help and technical support with the electron microprobe analyses and thin-section preparation. This work was carried out as part of M. S. Riishuus' Ph.D. project, financed by the Science Faculty at the University of Aarhus, with additional financial support from the defunct Danish Lithosphere Centre (financed by the Danish National Research Foundation). Finally, we thank Gregor Markl, Chris Harris, Stefan Bernstein and editor Marjorie Wilson for their thorough review of the manuscript.

REFERENCES

Ablay, G. J., Carroll, M. R., Palmer, M. R., Mart, J. & Sparks, R. S. J. (1998). Basanite–phonolite lineages of the Teide–Pico Viejo volcanic complex, Tenerife, Canary Islands. *Journal of Petrology* **39**, 905–936.

Andreasen, R., Peate, D. W. & Brooks, C. K. (2004). Magma plumbing systems in large igneous provinces: Inferences from cyclical variations in Palaeogene East Greenland basalts. *Contributions to Mineralogy and Petrology* **147**, 438–452.

Bailey, J. C., Gwozdz, R., Rose-Hansen, J. & Sørensen, H. (1978). Preliminary geochemical work on the Ilímaussaq alkaline intrusion, South Greenland. *Rapport Grønlands Geologiske Undersøgelse* **90**, 75–79.

Bailey, J. C., Sørensen, H., Andersen, T., Kogarko, L. N. & Rose-Hansen, J. (2006). On the origin of microrhythmic layering in arfvedsonite lujavrite from the Ilímaussaq alkaline complex, South Greenland. *Lithos* **91**, 301–318.

Baker, J., Peate, D., Waight, T. & Meyzen, C. (2004). Pb isotopic analysis of standards and samples using a ^{207}Pb–^{204}Pb double spike and thallium to correct for mass bias with a double-focusing MC-ICP-MS. *Chemical Geology* **211**, 275–303.

Bauer, K., Trumbull, R. B. & Vietor, T. (2003). Geophysical images and a crustal model of intrusive structures beneath the Messum ring complex, Namibia. *Earth and Planetary Science Letters* **216**, 65–80.

Beckinsale, R. D., Brooks, C. K. & Rex, D. C. (1970). K–Ar ages for the Tertiary of East Greenland. *Bulletin of the Geological Society of Denmark* **20**, 27–37.

Bernstein, S., Kelemen, P. B., Tegner, C., Kurz, M. D., Blusztajn, J. & Brooks, C. K. (1998). Post-breakup basaltic magmatism along the East Greenland Tertiary rifted margin. *Earth and Planetary Science Letters* **160**, 845–862.

Bindeman, I. N., Ponomareva, V. V., Bailey, J. C. & Valley, J. W. (2004). Volcanic arc of Kamchatka; a province with high-delta ^{18}O magma sources and large-scale $^{18}O/^{16}O$ depletion of the upper crust. *Geochimica et Cosmochimica Acta* **68**, 841–865.

Bizzarro, M., Baker, J. A. & Ulfbeck, D. (2003). A new digestion and chemical separation technique for rapid and highly reproducible determination of Lu/Hf and Hf isotope ratios in geological materials by MC-ICP-MS. *Geostandards Newsletter* **27**, 133–145.

Blundell, D. J. (1978). A gravity survey across the Gardar Igneous Province, SW Greenland. *Journal of the Geological Society, London* **135**, 545–554.

Bogaard, P. & Schmincke, H.-U. (1984). The eruptive center of the late Quaternary Laacher See tephra. *Geologische Rundschau* **73**, 935–982.

Brandriss, M. E., Bird, D. K., O'Neil, J. R. & Cullers, R. L. (1996). Dehydration, partial melting, and assimilation of metabasaltic xenoliths in gabbros of the Kap Edvard Holm Complex, East Greenland. *American Journal of Science* **296**, 333–393.

Brooks, C. K. & Gill, R. C. O. (1982). Compositional variation in the pyroxenes and amphiboles of the Kangerdlugssuaq intrusion, East Greenland: further evidence for the crustal contamination of syenite magma. *Mineralogical Magazine* **45**, 1–9.

Brooks, C. K. & Platt, R. G. (1975). Kaersutite-bearing gabbroic inclusions and the late dike swarm of Kangerdlugssuaq, East Greenland. *Mineralogical Magazine* **40**, 259–283.

Brown, P. E. (1973). A layered plutonic complex of alkali basalt parentage: the Lilloise intrusion, east Greenland. *Journal of the Geological Society, London* **129**, 405–418.

Chambers, A. D. & Brown, P. E. (1995). The Lilloise Intrusion, East Greenland—fractionation of a hydrous alkali picritic magma. *Journal of Petrology* **36**, 933–963.

Chen, J., Henderson, C. M. B. & Foland, K. A. (1994). Open-system, sub-volcanic magmatic evolution: constraints on the petrogenesis of the Mount Brome Alkaline Complex, Canada. *Journal of Petrology* **35**, 1127–1153.

Cohen, R. S. & O'Nions, R. K. (1982). The lead, neodymium and strontium isotopic structure of ocean ridge basalts. *Journal of Petrology* **23**, 299–324.

Dahl-Jensen, T., Larsen, T. B., Woelbern, I., Bach, T., Hanka, W., Kind, R., Gregersen, S., Mosegaard, K., Voss, P. & Gudmundsson, O. (2003). Depth to Moho in Greenland: receiver-function analysis suggests two Protorozoic blocks in Greenland. *Earth and Planetary Science Letters* **205**, 379–393.

Deer, W. A. & Kempe, D. R. C. (1976). Geological investigations in East Greenland, Part XI, The minor peripheral intrusions, Kangerdlugssuaq, East Greenland. *Meddelelser om Grønland* **197**, 1–25.

DePaolo, D. J. (1981). Trace element and isotopic effects of combined wallrock assimilation and fractional crystallisation. *Earth and Planetary Science Letters* **53**, 189–202.

Droop, G. T. R. (1987). A general equation for estimating Fe^{3+} concentrations in ferromagnesian silicates and oxides from microprobe analyses, using stoichiometric criteria. *Mineralogical Magazine* **51**, 431–435.

Elliott, T. R., Hawkesworth, C. J. & Grönvold, K. (1991). Dynamic melting of the Iceland plume. *Nature* **351**, 201–206.

Ferguson, J. (1964). Geology of the Ilímaussaq alkaline intrusion, south Greenland. *Bulletin Grønlands Geologiske Undersøgelse* **39**, 82.

Fitton, J. G. (1987). The Cameroon line, West Africa: a comparison between oceanic and continental alkaline volcanism. In: Fitton, J. G. & Upton, B. G. J. (eds) *Alkaline Igneous Rocks*. Oxford: Blackwell, pp. 273–291.

Foland, K. A. & Henderson, C. M. B. (1976). Application of age and Sr isotope data to the petrogenesis of the Marangudzi ring complex, Rhodesia. *Earth and Planetary Science Letters* **29**, 291–301.

Foland, K. A., Landoll, J. D., Henderson, C. M. B. & Chen, J. F. (1993). Formation of cogenetic quartz and nepheline syenites. *Geochimica et Cosmochimica Acta* **57**, 697–704.

Forsberg, R. & Rasmussen, K. L. (1978). Gravity and rock densities in the Ilímaussaq area, South Greenland. *Rapport Grønlands Geologiske Undersøgelse* **90**, 81–84.

Fram, M. S. & Lesher, C. E. (1997). Generation and polybaric differentiation of East Greenland early Tertiary flood basalts. *Journal of Petrology* **38**, 231–275.

Fudali, R. F. (1963). Experimental studies bearing on the origin of pseudoleucite and associated problems of alkalic rock systems. *Geological Society of America Bulletin* **74**, 1101–1126.

Furman, T., Frey, F. A. & Park, K.-H. (1991). Chemical constraint on the petrogenesis of mildly alkaline lavas from Vestmannaeyjar, Iceland: the Eldfell (1973) and Surtsey (1963–1967) eruptions. *Contributions to Mineralogy and Petrology* **109**, 19–37.

Giret, A., Bonin, B. & Leger, J. (1980). Amphibole compositional trends in oversaturated alkaline plutonic ring-complexes. *Canadian Mineralogist* **18**, 481–495.

Gleadow, A. J. W. & Brooks, C. K. (1979). Fission track dating, thermal histories and tectonics of igneous intrusions in East Greenland. *Contributions to Mineralogy and Petrology* **71**, 45–60.

Halama, R., Marks, M., Brugmann, G., Siebel, W., Wenzel, T. & Markl, G. (2004). Crustal contamination of mafic magmas: evidence from a petrological, geochemical and Sr–Nd–Os–O isotopic study of the Proterozoic Isortoq dike swarm, South Greenland. *Lithos* **74**, 199–232.

Hamilton, D. L. & MacKenzie, W. S. (1965). Phase-equilibrium studies in the system $NaAlSiO_4$ (nepheline)–$KAlSiO_4$ (kalsilite)–SiO_2–H_2O. *Mineralogical Magazine* **34**, 214–231.

Hanan, B. B. & Schilling, J.-G. (1997). The dynamic evolution of the Iceland mantle plume: the lead isotope perspective. *Earth and Planetary Science Letters* **151**, 43–60.

Hansen, H. & Nielsen, T. F. D. (1999). Crustal contamination in Palaeogene East Greenland flood basalts: plumbing system evolution during continental rifting. *Chemical Geology* **157**, 89–118.

Hansen, H., Pedersen, A. K., Duncan, R. A., Bird, D. K., Brooks, C. K., Fawcett, J. J., Gittins, J., Gorton, M. P. & O'Day, P. A. (2002). Volcanic stratigraphy of the southern Prinsen af Wales Bjerge region, East Greenland. In: Bell, B. R. (ed.) *The North Atlantic Igneous Province: Stratigraphy, Tectonic, Volcanic and Magmatic Processes. Geological Society, London, Special Publications* **197**, 183–218.

Hardarson, B. S., Fitton, J. G., Ellam, R. M. & Pringle, M. S. (1997). Rift relocation—a geochemical and geochronological investigation of a palaeo-rift in northwest Iceland. *Earth and Planetary Science Letters* **153**, 181–196.

Hards, V. L., Kempton, P. D. & Thompson, R. N. (1995). The heterogeneous Iceland plume: new insights from the alkaline basalts of the Snaefell volcanic centre. *Journal of the Geological Society, London* **152**, 1003–1009.

Harms, E. & Schmincke, H.-U. (2000). Volatile composition of the phonolitic Laacher See magma (12,900 yr BP): Implications for syneruptive degassing of S, F, Cl and H_2O. *Contributions to Mineralogy and Petrology* **138**, 84–98.

Harms, E., Gardner, J. E. & Schmincke, H.-U. (2004). Phase equilibria of the Lower Laacher See Tephra (East Eifel, Germany): Constraints on pre-eruptive storage conditions of a phonolitic magma reservoir. *Journal of Volcanology and Geothermal Research* **134**, 125–138.

Harris, C. (1995). Oxygen isotope geochemistry of the Mesozoic anorogenic complexes of Damaraland, northwest Namibia: evidence for crustal contamination and its effect on silica saturation. *Contributions to Mineralogy and Petrology* **122**, 308–321.

Harris, C., Marsh, J. S. & Milner, S. C. (1999). Petrology of the alkaline core of the Messum Igneous Complex, Namibia: Evidence for the progressively decreasing effect of crustal contamination. *Journal of Petrology* **40**, 1377–1397.

Holbrook, W. S., Larsen, H. C., Korenaga, J., Dahl-Jensen, T., Reid, I. D., Kelemen, P. B., Hopper, J. R., Kent, G. M., Lizarralde, D., Bernstein, S. & Detrick, R. S. (2001). Mantle thermal structure and active upwelling during continental breakup in the North Atlantic. *Earth and Planetary Science Letters* **190**, 251–266.

Holm, P. M. & Prægel, N.-O. (1988). The Tertiary Kærven Syenite Complex, Kangerdlugssuaq, East Greenland—mineral chemistry and geochemistry. *Mineralogical Magazine* **52**, 435–450.

Holm, P. M. & Prægel, N.-O. (2006). Cumulates from primitive rifting-related East Greenland Palaeogene magmas: petrological and isotopic evidence from the ultramafic complexes at Kælvegletscher and near Kærven. *Lithos* **92**, 251–275.

Kempe, D. R. C. & Deer, W. A. (1970). Geological investigations in East Greenland, part IX, The mineralogy of the Kangerdlugssuaq alkaline intrusion, East Greenland. *Meddelelser om Grønland* **190**, 1–97.

Kempe, D. R. C. & Deer, W. A. (1976). The petrogenesis of the Kangerdlugssuaq alkaline intrusion, East Greenland. *Lithos* **9**, 111–123.

Kempe, D. R. C., Deer, W. A. & Wager, L. R. (1970). Geological investigations in East Greenland, part VIII, The petrology of the Kangerdlugssuaq alkaline intrusion, East Greenland. *Meddelelser om Grønland* **190**, 1–52.

Kogarko, L. N. (1974). Role of volatiles. In: Sørensen, H. (ed.) *The Alkaline Rocks*. Chichester: John Wiley, pp. 474–487.

Kogarko, L. N. & Khapaev, V. (1987). The modelling of formation of apatite deposits of the Khibina massif (Kola Peninsula). In: Parsons, I. (ed.) *Origins of Igneous Layering. NATO ASI Series. Series C: Mathematical and Physical Sciences* **196**, 589–611.

Kogarko, L. N., Williams, C. T. & Woolley, A. R. (2002). Chemical evolution and petrogenetic implications of loparite in the layered, agpaitic Lovozero complex, Kola Peninsula, Russia. *Mineralogy and Petrology* **74**, 1–24.

Kogarko, L. N., Williams, C. T. & Woolley, A. R. (2006). Compositional evolution and cryptic variation in pyroxenes of the peralkaline Lovozero intrusion, Kola Peninsula, Russia. *Mineralogical Magazine* **70**, 347–359.

Korenaga, J., Holbrook, W. S., Kent, G. M., Kelemen, P. B., Detrick, R. S., Larsen, H. C., Hopper, J. R. & Dahl-Jensen, T. (2000). Crustal structure of the southeast Greenland margin from joint refraction and reflection seismic tomography. *Journal of Geophysical Research* **105**, 21591–21614.

Kramm, U. & Kogarko, L. N. (1994). Nd and Sr isotope signatures of the Khibina and Lovozero agpaitic centres, Kola Alkaline Province, Russia. *Lithos* **32**, 225–242.

Kyle, P. R. (1981). Mineralogy and geochemistry of a basanite to phonolite sequence at Hut Point peninsula, Antarctica, based on core from Dry Valley Drilling Project drillholes 1, 2 and 3. *Journal of Petrology* **22**, 451–500.

Landoll, J. D., Foland, K. A. & Henderson, C. M. B. (1994). Nd isotopes demonstrate the role of contamination in the formation of coexisting quartz and nepheline syenites at the Abu-Khruq complex, Egypt. *Contributions to Mineralogy and Petrology* **117**, 305–329.

Larsen, L. M. & Sørensen, H. (1987). The Ilímaussaq intrusion—progressive crystallization and formation of layering in an agpaitic magma. In: Fitton, J. G. & Upton, B. G. J. (eds) *Alkaline Igneous Rocks. Geological Society, London, Special Publications* **30**, 489–515.

Larsen, L. M. & Watt, W. S. (1985). Episodic volcanism during breakup of the North Atlantic: evidence from the East Greenland plateau basalts. *Earth and Planetary Science Letters* **73**, 105–116.

Larsen, L. M., Watt, W. S. & Watt, M. (1989). Geology and petrology of the lower Tertiary plateau basalts of the Scoresby Sund region, East Greenland. *Geological Survey of Greenland Bulletin* **157**, 1–164.

Larsen, R. B. & Tegner, C. (2006). Pressure conditions for the solidification of the Skaergaard: Eruption of East Greenland flood basalts in less than 300,000 years. *Lithos* **92**, 181–197.

Leake, B. E., Woolley, A. R., Arps, C. E. S. *et al.* (1997). Nomenclature of amphiboles: report of the subcommittee on amphiboles of the international mineralogical association, commission on new minerals and mineral names. *Canadian Mineralogist* **35**, 219–246.

Le Bas, M. J. & Streckeisen, A. L. (1991). The IUGS systematics of igneous rocks. *Journal of the Geological Society, London* **148**, 825–833.

Leeman, W. P., Dasch, E. J. & Kays, M. A. (1976). $^{207}Pb/^{206}Pb$ whole-rock ages of gneisses from the Kangerdlugssuaq area, eastern Greenland. *Nature* **263**, 469–471.

Le Maitre, R. W. (ed.) (2005). *A Classification of Igneous Rocks and Glossary of Terms*. Oxford: Blackwell, 256 p.

leRoex, A. P., Cliff, R. A. & Adair, B. J. I. (1990). Tristan da Cunha, South Atlantic: geochemistry and petrogenesis of a basanite–phonolite lava series. *Journal of Petrology* **31**, 779–812.

Lynton, S. J., Candela, P. A. & Piccoli, P. M. (1993). An experimental study of the partitioning of copper between pyrhotite and a high silica rhyolitic melt. *Economic Geology and the Bulletin of the Society of Economic Geologists* **88**, 901–915.

Markl, G., Marks, M., Schwinn, G. & Sommer, H. (2001). Phase equilibrium constraints on intensive crystallization parameters of the Ilímaussaq complex, South Greenland. *Journal of Petrology* **42**, 2231–2258.

Marks, M. & Markl, G. (2001). Fractionation and assimilation processes in the alkaline augite syenite unit of the Ilímaussaq intrusion, South Greenland, as deduced from phase equilibria. *Journal of Petrology* **42**, 1947–1969.

Marks, M., Vennemann, T., Siebel, W. & Markl, G. (2003). Quantification of magmatic and hydrothermal processes in a peralkaline syenite–alkali granite complex based on textures, phase equilibria, and stable and radiogenic isotopes. *Journal of Petrology* **44**, 1247–1280.

Marks, M., Vennemann, T., Siebel, W. & Markl, G. (2004). Nd-, O-, and H-isotopic evidence for complex, closed-system fluid evolution of the peralkaline Ilímaussaq intrusion, South Greenland. *Geochimica et Cosmochimica Acta* **68**, 3379–3395.

McDonough, W. F. & Sun, S.-s. (1995). The composition of the Earth. *Chemical Geology* **120**, 223–253.

Morse, S. A. (1969). Syenites. *Carnegie Institution of Washington Annual Report Geophysical Laboratory* **67**, 112–120.

Nielsen, F. M., Campbell, I. H., McCulloch, M. & Wilson, J. R. (1996). A strontium isotopic investigation of the Bjerkreim–Sokndal layered intrusion, southwest Norway. *Journal of Petrology* **37**, 171–193.

Nielsen, T. F. D. (1978). The Tertiary dike swarms of the Kangerdlugssuaq area, East Greenland. An example of magmatic development during continental break-up. *Contributions to Mineralogy and Petrology* **67**, 63–78.

Nielsen, T. F. D. (1980). The petrology of a melilitolite, melteigite, carbonatite and syenite ring dike system in the Gardiner Complex, East Greenland. *Lithos* **13**, 181–197.

Nielsen, T. F. D. (1981). The ultramafic cumulate series, Gardiner Complex, East Greenland—cumulates in a shallow level magma chamber of a nephelinitic volcano. *Contributions to Mineralogy and Petrology* **76**, 60–72.

Nielsen, T. F. D. (1987). Tertiary alkaline magmatism in East Greenland: a review. In: Fitton, J. G. & Upton, B. G. J. (eds) *Alkaline Igneous Rocks. Geological Society, London, Special Publications* **30**, 489–515.

Nielsen, T. F. D. (2002). Palaeogene intrusions and magmatic complexes in East Greenland, 66 to 75° N. *Geological Survey of Denmark and Greenland Report* **2002/113**, 249 pp.

Nielsen, T. F. D., Soper, N. J., Brooks, C. K., Faller, A. M., Higgins, A. C. & Matthews, D. W. (1981). The pre-basaltic sediments and the Lower Basalts at Kangerdlugssuaq, East Greenland: their stratigraphy, lithology, palaeomagnetism and petrology. *Meddelelser om Grønland, Geoscience* **6**, 1–25.

Nielsen, T. F. D., Hansen, H., Brooks, C. K., Lesher, C. E. & field parties, (2001). The East Greenland continental margin, the Prinsen af Wales Bjerge and new Skaergaard intrusion initiatives. *Geology of Greenland Survey Bulletin* **189**, 83–98.

Pankhurst, R. J., Beckinsale, R. D. & Brooks, C. K. (1976). Strontium and oxygen isotope evidence relating to the petrogenesis of the Kangerdlugssuaq alkaline intrusion, East Greenland. *Contributions to Mineralogy and Petrology* **54**, 17–42.

Park, K. H. (1990). *Sr, Nd and Pb Isotope Studies of Ocean Island Basalts: Constraints on their Origin and Evolution*. New York: Columbia University, 252 p.

Parsons, I. (1979). Klokken gabbro–syenite complex, South Greenland—cryptic variation and origin of inversely graded layering. *Journal of Petrology* **20**, 653–694.

Parsons, I. & Becker, S. M. (1987). Layering, compaction and postmagmatic processes in the Klokken intrusion. In: Parsons, I. (ed.) *Origins of Igneous Layering. NATO ASI Series. Series C: Mathematical and Physical Sciences* **196**, 29–92.

Pearce, N. J. G., Perkins, W. T., Westgate, J. A., Gorton, M. P., Jackson, S. E., Neal, C. R. & Chenery, S. P. (1997). A compilation of new and published major and trace element data for NIST SRM 610 and NIST SRM 612 glass reference materials. *Geostandards Newsletter* **21**, 115–144.

Peate, D. W. & Stecher, O. (2003). Pb isotope evidence for contributions from different Iceland mantle components to Palaeogene East Greenland flood basalts. *Lithos* **67**, 39–52.

Peate, D. W., Baker, J. A., Blichert-Toft, J., Hilton, D. R., Storey, M., Kent, A. J. R., Brooks, C. K., Hansen, H., Pedersen, A. K. & Duncan, R. A. (2003). The Prinsen af Wales Bjerge Formation lavas, East Greenland: the transition from tholeiitic to alkalic magmatism during Palaeogene continental break-up. *Journal of Petrology* **44**, 279–304.

Pedersen, A. K., Watt, M., Watt, W. S. & Larsen, L. M. (1997). Structure and stratigraphy of the early Tertiary basalts of the Blosseville Kyst, East Greenland. *Journal of the Geological Society, London* **154**, 565–570.

Petersen, J. S. (1978). Structure of the larvikite–ladarlite complex, Oslo-region, Norway, and its evolution. *Geologische Rundschau* **67**, 330–342.

Petersen, J. S. (1985). Columnar–dendritic feldspars in the Lardalite Intrusion, Oslo region, Norway: 1. Implications for unilateral solidification of a stagnant boundary layer. *Journal of Petrology* **26**, 223–252.

Ramberg, I. B. & Smithson, S. B. (1971). Gravity interpretation of the southern Oslo Graben and adjacent Precambrian rocks, Norway. *Tectonophysics* **11**, 419–431.

Riishuus, M. S., Peate, D. W., Tegner, C., Wilson, J. R., Brooks, C. K. & Waight, T. E. (2005). Petrogenesis of syenites at a rifted continental margin: origin, contamination and interaction of alkaline mafic and felsic magmas in the Astrophyllite Bay Complex, East Greenland. *Contributions to Mineralogy and Petrology* **149**, 350–371.

Riishuus, M. S., Peate, D. W., Tegner, C., Wilson, J. R., Brooks, C. K. & Harris, C. (2006). Temporal evolution of a long-lived syenitic centre: the Kangerlussuaq Alkaline Complex, East Greenland. *Lithos* **92**, 276–299.

Saunders, A. D., Fitton, J. G., Kerr, A. C., Norry, M. J. & Kent, R. W. (1997). The North Atlantic Igneous Province. In: Mahoney, J. J. & Coffin, M. F. (eds) *Large Igneous Provinces: Continental, Oceanic, and Planetary Flood Volcanism. Geophysical Monograph, American Geophysical Union* **100**, 45–93.

Schairer, J. F. (1950). The alkali–feldspar join in the system $NaAlSiO_4$–$KAlSiO_4$–SiO_2. *Journal of Geology* **58**, 512–517.

Schmitt, A. K., Emmermann, R., Trumbull, R. B., Bühn, B. & Henjes-Kunst, F. (2000). Petrogenesis and $^{40}Ar/^{39}Ar$ geochronology of the Brandberg Complex, Namibia: Evidence for a major mantle contribution in metaluminous and peralkaline granites. *Journal of Petrology* **41**, 1207–1239.

Stephenson, D. & Upton, B. G. J. (1982). Ferromagnesian silicates from a differentiated alkaline complex: Kûngnât Fjeld, South Greenland. *Mineralogical Magazine* **46**, 283–300.

Stevenson, R., Upton, B. G. J. & Steenfelt, A. (1997). Crust–mantle interaction in evolution of the Ilímaussaq Complex, South Greenland: Nd isotopic studies. *Lithos* **40**, 189–202.

Sørensen, H. & Larsen, L. M. (1987). Layering in the Ilímaussaq alkaline intrusion, South Greenland. In: Parsons, I. (ed.) *Origins of Igneous Layering. NATO ASI Series. Series C: Mathematical and Physical Sciences* **196**, 1–28.

Sørensen, H. S. & Wilson, J. R. (1995). A strontium and neodymium isotopic investigation of the Fongen–Hyllingen layered intrusion, Norway. *Journal of Petrology* **36**, 161–187.

Stecher, O., Carlson, R. W. & Gunnarsson, B. (1999). Torfajokull: a radiogenic end-member of the Iceland Pb-isotopic array. *Earth and Planetary Science Letters* **165**, 117–127.

Storey, M., Pedersen, A. K., Stecher, O., Bernstein, S., Larsen, H. C., Larsen, L. M., Baker, J. A. & Duncan, R. A. (2004). Long-lived postbreakup magmatism along the East Greenland margin: evidence for shallow-mantle metasomatism by the Iceland plume. *Geology* **32**, 173–176.

Storey, M., Duncan, R. A. & Tegner, C. (2007). Timing and duration of volcanism in the North Atlantic Igneous Province: implications for geodynamics and links to the Iceland hotspot. *Chemical Geology* **241**, 264–281.

Sun, S.-S. & Jahn, B.-M. (1975). Lead and strontium isotopes in postglacial basalts from Iceland. *Nature* **255**, 527–530.

Sun, S.-S., Tatsumoto, M. & Schilling, J.-G. (1975). Mantle plume mixing along the Reykjanes Ridge axis: lead isotope evidence. *Science* **190**, 143–147.

Taylor, P. N., Kalsbeek, F. & Bridgwater, D. (1992). Discrepancies between neodymiun, lead and strontium model ages from the Precambrian of southern East Greenland: evidence for a Proterozoic granulite-facies event affecting Archaean gneisses. *Chemical Geology (Isotope Geoscience Section)* **94**, 281–291.

Tegner, C., Duncan, R. A., Bernstein, S., Brooks, C. K., Bird, D. K. & Storey, M. (1998*a*). ^{40}Ar–^{39}Ar geochronology of Tertiary mafic intrusions along the East Greenland rifted margin: Relation to flood basalts and the Iceland hotspot track. *Earth and Planetary Science Letters* **156**, 75–88.

Tegner, C., Lesher, C. E., Larsen, L. M. & Watt, W. S. (1998*b*). Evidence from the rare-earth-element record of mantle melting for cooling of the Tertiary Iceland plume. *Nature* **395**, 591–594.

Tegner, C., Robins, B., Reginiussen, H. & Grundvig, S. (1999). Assimilation of crustal xenoliths in a basaltic magma chamber: Sr and Nd isotopic constraints from the Hasvik Layered Intrusion, Norway. *Journal of Petrology* **40**, 363–380.

Tegner, C., Brooks, C. K., Duncan, R. A., Heister, L. E. & Bernstein, S. (2008). ^{40}Ar–^{39}Ar ages of intrusions in East Greenland: Rift-to-drift transition over the Iceland hotspot. *Lithos* doi:10.1016/j.lithos.2007.09.001.

Thompson, G. M., Smith, I. E. M. & Malpas, J. G. (2001). Origin of oceanic phonolites by crystal fractionation and the problem of the Daly gap: an example from Rarotonga. *Contributions to Mineralogy and Petrology* **142**, 336–346.

Tuttle, O. F. & Bowen, N. L. (1958). *Origin of Granite in the Light of Experimental Studies in the System NaAlSiO4–KAlSiO4–SiO2–H2O. Geological Society of America, Memoirs* **74**, 1–153.

Ulfbeck, D., Baker, J., Waight, T. & Krogstad, E. (2003). Rapid sample digestion by fusion and chemical separation of Hf for isotopic analysis by MC-ICPMS. *Talanta* **59**, 365–373.

Upton, B. G. J. (1987). Gabbroic, syenogabbroic and syenitic cumulates of the Tugtutôq Younger Giant Dyke Complex, South Greenland. In: Parsons, I. (ed.) *Origins of Igneous Layering. NATO ASI Series. Series C: Mathematical and Physical Sciences* **196**, 93–123.

Upton, B. G. J., Stephenson, D. & Martin, A. R. (1985). The Tututoq Older Giant Dyke Complex: Mineralogy and geochemistry of an alkali gabbro–augite syenite–foyaite association in the Gardar Province of South Greenland. *Mineralogical Magazine* **49**, 623–642.

Upton, B. G. J., Emeleus, C. H., Heaman, L. M., Goodenough, K. M. & Finch, A. A. (2003). Magmatism of the mid-Proterozoic Gardar Province, South Greenland: chronology, petrogenesis and geological setting. *Lithos* **68**, 43–65.

Verhoef, J., Roest, W. R., Macnab, R. & Arkani-Hamed, J. (1996). *Magnetic anomalies of the Arctic and North Atlantic oceans and adjacent land areas. Geological Survey of Canada, Open File* **3125**.

Villemant, B. (1988). Trace element evolution in the Plegrean Fields, Central Italy: fractional crystallization and selective enrichment. *Contributions to Mineralogy and Petrology* **98**, 169–183.

Wager, L. R. (1965). The form and internal structure of the alkaline Kangerdlugssuaq intrusion, East Greenland. *Mineralogical Magazine* **34**, 487–497.

Waight, T., Baker, J. & Willigers, B. (2002). Rb isotope dilution analyses by MC-ICPMS using Zr to correct for mass fractionation: towards improved Rb–Sr geochronology? *Chemical Geology* **186**, 99–116.

Wörner, G. & Schmincke, H.-U. (1984). Petrogenesis of the zoned Laacher See Tephra. *Journal of Petrology* **25**, 836–851.

Wörner, G. & Wright, T. L. (1984). Evidence for magma mixing within the Laacher See magma chamber (East Eifel, Germany). *Journal of Volcanology and Geothermal Research* **22**, 301–327.